Understanding and Targeting Coronaviruses: exploring advanced cell culture models and host-directed antiviral strategies

Thaler, M.

Chapter 2

Impact of Changes in human airway epithelial cellular composition and differentiation on SARS-CoV-2 infection biology

Melissa Thaler[1]*, Ying Wang[2]*, Anne M. van der Does[2], Alen Faiz[3], Dennis K. Ninaber[2], Natacha S. Ogando[1], Hendrik Beckert[4], Christian Taube[4], Clarisse Salgado-Benvindo[1], Eric J. Snijder[1], Peter J. Bredenbeek[1], Pieter S. Hiemstra[2#], Martijn J. van Hemert[1#]

[1] Department of Medical Microbiology, Leiden University Medical Center, Leiden, The Netherlands
[2] Department of Pulmonology, Leiden University Medical Center, Leiden, The Netherlands
[3] University of Technology Sydney, Respiratory Bioinformatics and Molecular Biology (RBMB), School of Life Sciences, Sydney, Australia
[4] Department of Pulmonary Medicine, University Medical Center Essen – Ruhrlandklinik, Essen, Germany

* These authors share first authorship
# These authors share senior authorship

Journal of Innate Immunity (2023) 15 (1): 562–580

Abstract

The consequences of infection with severe acute respiratory syndrome coronavirus 2 (SARS-CoV-2) can range from asymptomatic to fatal disease. Variations in epithelial susceptibility to SARS-CoV-2 infection depend on the anatomical location from the proximal to distal respiratory tract. However, the cellular biology underlying these variations is not completely understood. Thus, air-liquid interface (ALI) cultures of well-differentiated primary human tracheal and bronchial epithelial cells were employed to study the impact of epithelial cellular composition and differentiation on SARS-CoV-2 infection by transcriptional (RNA sequencing) and immunofluorescent analyses. Changes of cellular composition were investigated by varying time of differentiation or by using specific compounds. We found that SARS-CoV-2 primarily infected ciliated cells but also goblet cells and transient secretory cells. Viral replication was impacted by differences in cellular composition, which depended on culturing time and anatomical origin. A higher percentage of ciliated cells correlated with a higher viral load. However, DAPT-treatment, which increased number of ciliated cells and reduced goblet cells, decreased viral load, indicating the contribution of goblet cells to infection. Cell-entry factors, especially cathepsin L and transmembrane protease serine 2, were also affected by differentiation time. In conclusion, our study demonstrates that viral replication is affected by changes in cellular composition, especially in cells related to the mucociliary system. This could explain in part the variable susceptibility to SARS-CoV-2 infection between individuals and between anatomical locations in the respiratory tract.

Introduction

Since December 2019, severe acute respiratory syndrome coronavirus 2 (SARS-CoV-2) has rapidly spread worldwide. The burden of the associated coronavirus disease 2019 (COVID-19) has an enormous medical, social and economic impact (211). Furthermore, the continuing emergence of virus variants, such as the delta and omicron variants, are associated with additional waves of COVID-19 cases (212, 213). This illustrates the threat of these viruses to prolong the current pandemic or lead to new large outbreaks in the future. Besides different clinical outcomes due to SARS-CoV-2 variants, even people infected with the same virus variant present with varying clinical signs and symptoms depending on age (214), sex (215), weight (216), environment (217), other medical conditions (216, 218), immune status (219), and possibly other yet to be identified factors.

SARS-CoV-2 was first isolated from the lower respiratory tract of COVID-19 patients (15, 220). The epithelium serves as the first barrier to SARS-CoV-2 infection in the respiratory tract and therefore the subsequent epithelial response to infection (antiviral and

inflammatory responses) plays an important role in the outcome of infection. The respiratory tract spans from the nasal cavity to the terminal bronchioles, ending in the alveoli where gas exchange occurs. The airways are lined by the airway epithelium, which includes various cell types, of which ciliated, secretory goblet and club cells, and basal cells are present in the highest numbers (221, 222). These cell types have their own distinct functions. For instance, goblet cells secrete mucus, which captures inhaled particles like respiratory viruses, while the continuous beating cilia from ciliated cells help to transport this mucus with entrapped particles towards the pharynx, collectively called mucociliary clearance (MCC). Although the airway epithelium shares similar cell types throughout the respiratory tract, the proportion of each cell type is dependent on the anatomical location (223). In addition, in many patients with lung diseases such as asthma or chronic obstructive pulmonary disease (COPD), epithelial cellular composition is altered (222). In primary airway epithelial cell cultures, which are differentiated at the air-liquid interface (ALI), cellular composition of the airway epithelium depends on the individual donor (224), differentiation time (131), and culture conditions (133). So far, the impact of epithelial cellular composition on SARS-CoV-2 infection biology has not been completely elucidated. Previous studies have demonstrated a difference in host susceptibility to SARS-CoV-2 infection depending on the location of virus-host interaction in the respiratory tract (225). However, it is unclear to what extent the differences in viral replication link to variation in epithelial cellular composition. SARS-CoV-2 targets ciliated and secretory cells (71, 226), possibly via strands of mucus attached to cilia tips (227). Therefore, changes in the proportion of these target cells might affect viral replication. SARS-CoV-2 cellular tropism furthermore depends on host proteins that are involved in virus entry, including angiotensin converting enzyme 2 (ACE2) and proteases like transmembrane protease serine 2 (TMPRSS2) and cathepsin L (CTSL), as well as alternative receptors (e.g. cluster of differentiation 147 [CD147], 78-kDa glucose-regulated protein [GRP78], tyrosine-protein kinase receptor UFO [AXL]), which all have been demonstrated to be expressed in variable levels on human airway epithelial cells (45, 228-230). Recent research demonstrated that SARS-CoV-2 cell-entry factors are primarily expressed in bronchial transient secretory cells (231), indicating these transiently differentiating cells might contribute to a great extent to initial infection.

While research on the susceptibility of respiratory epithelial cells to SARS-CoV-2 infection often focuses on a specific cell-type, function or protein of interest (232), we aimed to investigate how various changes in cellular differentiation and composition affect SARS-CoV-2 infection biology. This knowledge can support our understanding of how these factors could contribute to local, and - more importantly - airway disease-associated differences in susceptibility. To this end, we used primary human bronchial (PBEC) and tracheal epithelial cells (PTEC) and differentiated them at the air-liquid interface (ALI) for up

to 5 weeks. We characterized virus replication, spread, localization, immune responses, and expression of SARS-CoV-2-entry factors, as well as compared cellular composition between both types of cultures. Furthermore, we investigated how infection characteristics were influenced by modulation of the cellular composition and by the duration of culture.

Results

Susceptibility of airway epithelial cultures to SARS-CoV-2 differs between individual donors

To investigate the effect of differentiation status and cellular composition of the airway epithelium on SARS-CoV-2 infection biology, we first aimed to establish a reliable infection model. We investigated donor-dependent variability in infection by comparing SARS-CoV-2 replication kinetics in cultures of 4 individual donors and a mix of those donors. Between the single donor cultures, we observed some variation in viral load (**Figure 1a**). Cultures derived from mixes of primary cells from these donors (donor mix) showed comparable infection kinetics with regard to this variation, and immunofluorescence staining confirmed similar numbers of infected cells at 72 hours post infection (hpi) for single donors and donor mix (**Figure 1b**). Thus ALI-PBEC cultures of mixed donor cells proved to be a representative model to investigate characteristics of airway epithelial cell cultures and to test many variables, while keeping sample size relatively limited.

We performed infections at a relatively low multiplicity of infection (MOI) to model the initial stage of infection by initially only infecting a fraction of susceptible cells and observe the virus spread across the epithelium over time. Four independent experiments were performed using ALI-PBEC derived from the same donor mix. After infection with SARS-CoV-2 (estimated 30,000 PFU per insert), we observed an increase in viral load (extracellular copies of viral RNA) over time, to approximately 10^{11} copies/ml at 72 hpi (**Figure 1c**). Immunofluorescence staining of the epithelial cultures for viral nucleocapsid protein also showed a gradual increase in the number of infected cells over time (**Figure 1d**). The number of infected cells was low and generally detected at the edge of the insert (**Figure S1a**) as also previously reported (233).

To validate the relevance of our cell culture model for studying epithelial defence against SARS-CoV-2 infection, we measured antiviral responses (IFN-β1 and IFN-λ1) and inflammatory cytokines (IL-6 and IL-8 [CXCL8]) (**Figure S1**). We observed that SARS-CoV-2 infection did not affect mRNA levels of *IFNB1* and *IFNL1* at 24 and 48 h, but strongly increased their expression at 72 hpi (**Figure S1b**). At 72 hpi, mRNA levels of both *IL6* and *CXCL8* displayed a modest but significant increase in SARS-CoV-2-infected cultures (**Figure**

S1c). We established reproducible and robust infection kinetics in this model, accompanied by a significant but late epithelial antiviral and inflammatory response that is characteristic for SARS-CoV-2 infection (234).

SARS-CoV-2 primarily infects epithelial cells involved in mucociliary clearance

Previous studies have indicated that within the human respiratory tract, predominantly ciliated cells, but also goblet cells of the airway epithelium can be infected with SARS-CoV-2 (226), as well as alveolar epithelial cells (138, 235). To assess if ciliated and goblet cells were also the target cells in our cultures, we investigated the colocalization of SARS-CoV-2 nucleocapsid protein with either acetylated α-tubulin and FOXJ1 as markers for ciliated cells, or MUC5AC as a marker for goblet cells. Recently, a new transient secretory cell subtype which is positive for markers of ciliated and goblet cells, was suggested to be particularly susceptible to SARS-CoV-2 based on ACE2 and TMPRSS2 expression (236). We observed presence of most of the viral nucleocapsid protein in acetylated α-tubulin-positive ciliated cells in ALI-PBEC cultures, with less presence in $MUC5AC^+$ goblet cells (**Figure 1e**), showing that both cell types can indeed be infected by SARS-CoV-2. Additionally, immunofluorescence staining showed that few transient secretory cells - defined as FOXJ1 and MUC5AC double-positive cells - were present and infected by SARS-CoV-2 (**Figure 1f**).
We next investigated if the number of SARS-CoV-2 target cells in the single donor cultures depicted in **Figure 1a**, correlated with the level of infection. Interestingly, quantification by immunofluorescence staining showed that cultures from donor 3, which had the higher initial viral load (at 24 hpi) compared to cells from donor 1 with the lowest initial viral load, constituted a higher proportion of $FOXJ1^+$ ciliated cells, as well as transient secretory cells (**Figure 1g**). This result suggests that the differences in susceptibility of cultures from different donors to viral infection might be associated with variation in the percentages of the different SARS-CoV-2 target cells.

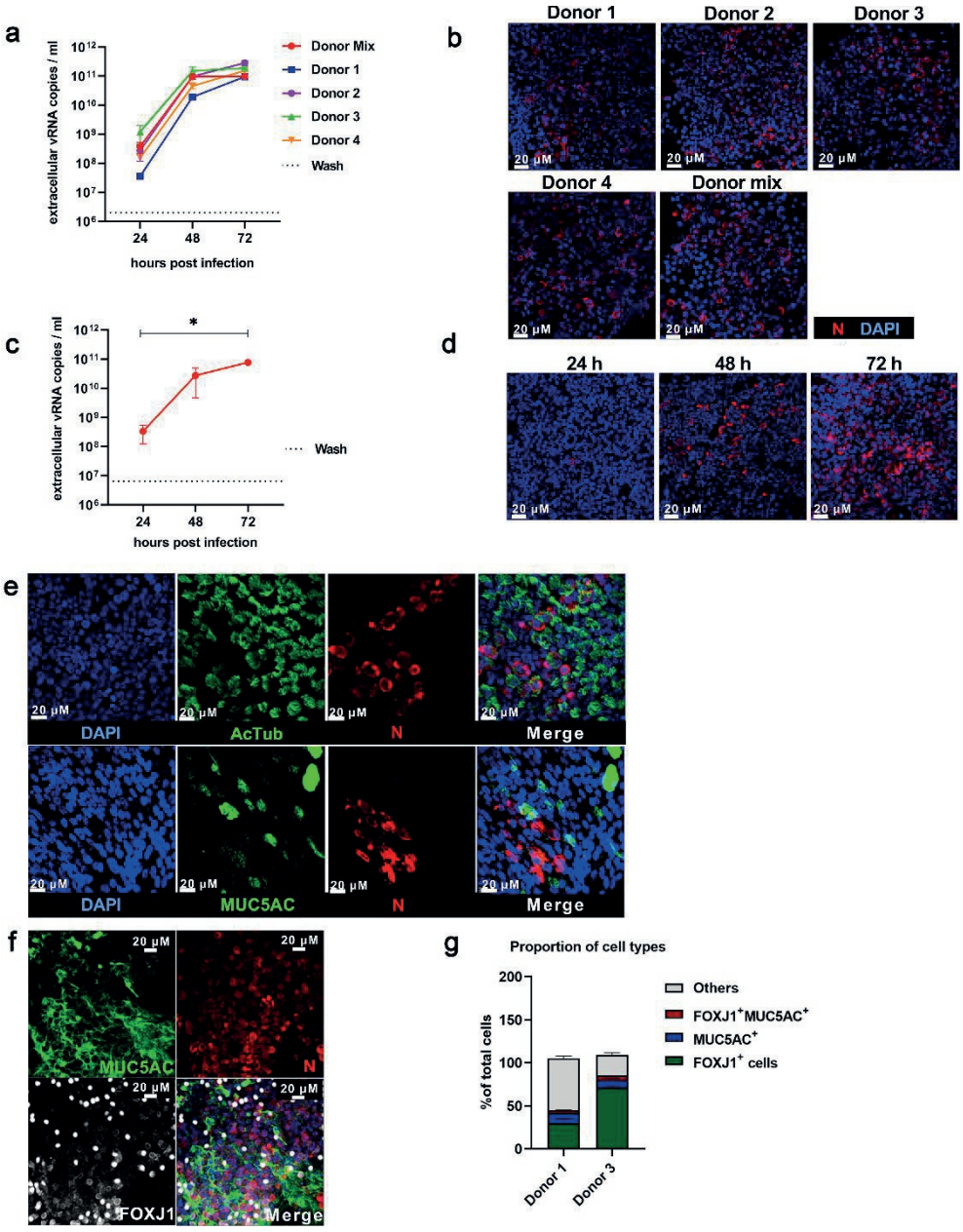

Figure 1: Characterization of a SARS-CoV-2 infection model using air-liquid interface cultures of primary bronchial epithelial cells. Mixes of PBEC derived from 4-5 individual donors were cultured for 5 weeks at ALI before they were infected with SARS-CoV-2 (30,000 PFU per insert). (a) The viral load in cultures derived from single donors or a mix of these donors (in red) was determined by quantifying the level of extracellular viral RNA copies by RT-qPCR. The dashed line represents the amount of (input) viral RNA that remained in the last wash after washing the inserts at 2 hpi (mean of all donors). (b) The infected cells were stained with rabbit polyclonal anti-

SARS-CoV-2 N protein antibody (JUC3) and with 4',6-diamidino-2-phenylindole (DAPI), and visualized by immunofluorescence microscopy at 72 hpi. Images shown at 400 x original magnification are representative merged z-stack images for results obtained with cells from random areas of the inserts. (c) The viral load at 24, 48 and 72 hpi in cultures was determined by quantifying the number of extracellular viral RNA copies by RT-qPCR. Data are mean ± SEM. n=4 independent experiments with the same donor mix. (d) For immunofluorescence microscopy, cells were fixed at 72 hpi and (double) labelled with rabbit polyclonal anti-SARS-CoV-2 N protein antibody (JUC3) and with DAPI for nuclear staining. Images shown at 400 x original magnification are representative merged z-stack images for results obtained with cells from 3 independent experiments. (e) Immunofluorescence staining at 72 hpi, with antibodies against acetylated α-tubulin (ciliated cell marker) or MUC5AC (goblet cell marker) in combination with anti-SARS-CoV-2 N protein antibody (JUC3) and DAPI for nuclear staining. Immunofluorescence images shown are representative merged z-stack images for results of 3 independent experiments with 630 x original magnification. (f) Immunofluorescence staining with antibodies against MUC5AC and FOXJ1 (ciliated cell marker) with anti-SARS-CoV-2 N protein antibody and DAPI for nuclear staining. Immunofluorescence images shown are representative merged z-stack images for results of 3 independent experiments with 400 x original magnification. (g) Quantification of immunostaining of $FOXJ1^+$, $MUC5AC^+$ and $FOXJ1^+MUC5AC^+$ or other cells in cultures of two single donors was performed with Image J software.

Modulating epithelial cellular composition has moderate effects on SARS-CoV-2 infection

To further explore the association between epithelial cellular composition and viral infection, we skewed cellular differentiation of ALI-PBEC during the last 2 weeks of differentiation to either an enrichment in ciliated cells at the cost of goblet cells, or towards an enrichment in goblet cells at the expense of ciliated cells using DAPT or interleukin 13 (IL-13), respectively (237-239). We infected these cultures with SARS-CoV-2 to analyse if enrichment in one of these cell types impacted infection kinetics. We could verify that DAPT treatment caused a marked increase in the number of ciliated cells ($FOXJ1^+$ and acetylated α-$tubulin^+$), while the number of goblet cells ($MUC5AC^+$) was decreased (**Figure 2a** and **S2a**). Conversely, IL-13 treatment increased the fraction of goblet cells and decreased the number of ciliated cells (**Figure 2A** and **S2A**), also confirmed at gene expression level (**Figure S2b**). Additionally, a small percentage of FOXJ1 and MUC5AC double-positive transient secretory cells was detected in all cultures, which was not significantly affected by IL-13 or DAPT treatment (**Figure S2a**).

We infected these DAPT- or IL-13-treated cultures with SARS-CoV-2 and in line with the data shown in **Figure 1**, detected by immunofluorescence staining that only a few cells were infected at 24 hpi in untreated and treated cultures (**Figure 2b**). At 48 and 72 hpi, all cultures showed an increase in viral load compared to 24 hpi (**Figure 2b**), demonstrating that viral infection and replication was feasible in all cultures despite the significant change in cellular composition between these conditions. In IL-13-treated cell cultures, intracellular viral RNA levels were highest at 48 hpi, while being similar to control again at 72 hpi (**Figure 2c**). To

our surprise the level of intracellular SARS-CoV-2 RNA was lower in DAPT-treated cells at all time points compared to the controls (**Figure 2c**). Similar trends were found for the release of infectious particles, as shown in **Figure 2d**. When we checked for cell types infected with SARS-CoV-2 in DAPT-treated cultures, due to the lack of goblet cells, ciliated cells were the only identified cells. In IL-13-treated cultures we observed infection of ciliated and goblet cells, similar to control cultures. (**Figure 2e**).

To exclude the possibility that the effects observed in DAPT-treated cultures were a direct consequence of inhibition of Notch signalling rather than epithelial remodelling, we treated cells with DAPT either starting 24 h before (and during) infection (a time period considered insufficient to cause a shift in epithelial differentiation) or directly after infection. These short-term treatments with DAPT did not result in significant changes in the intracellular viral RNA copies or production of infectious progeny, suggesting that inhibition of Notch signalling itself has no direct effect on SARS-CoV-2 replication (**Figure S2c**). These data suggest that rather than one cell-type alone, possibly the interplay between goblet and ciliated cells is important for susceptibility of ALI-PBEC to SARS-CoV-2 infection.

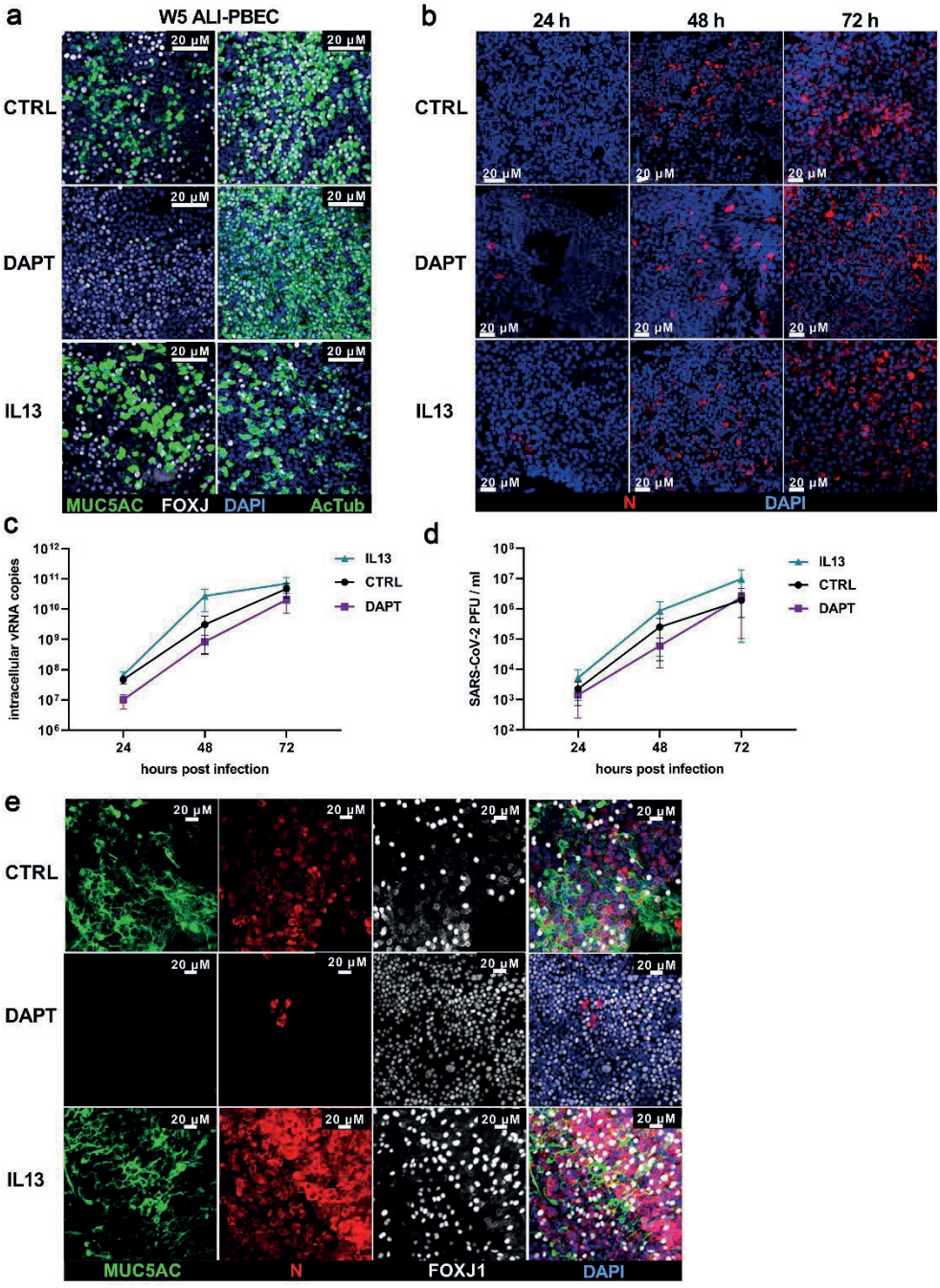

Figure 2: Effect of IL-13 treatment, and DAPT-mediated inhibition of Notch signaling on epithelial susceptibility to SARS-CoV-2 infection. ALI-PBEC (mix of 4-5 donors) were differentiated for 3 weeks, before addition of DAPT (5 µM) or IL-13 (1 ng/ml) and differentiation for an additional 2 weeks. (a) After in total 5 weeks of differentiation,

ALI-PBEC were fixed, stained using primary antibodies against MUC5AC and FOXJ1 (goblet cell marker, ciliated cell marker) or acetylated α-tubulin together with FOXJ1 (ciliated cell markers) in combination with DAPI for nuclear staining, analyzed by immunofluorescence microscopy and quantified by ImageJ. Immunofluorescence images shown are representative merged z-stack images for results of 3 independent experiments with 400 x original magnification. (b) SARS-CoV-2 infected cells were stained with primary antibodies against SARS-CoV-2 N protein (JUC3) in combination with DAPI for nuclear staining. Immunofluorescence images shown are representative merged z-stack images for results of 3 independent experiments with 400 x original magnification. (c) Intracellular viral RNA copies were measured by RT-qPCR. (d) Plaque assay was performed to titrate viral progeny in the apical washes. n=3 independent experiments derived from 3 different donor mixes. Data are mean ± SEM. Analysis of differences was conducted using two-way ANOVA with a Tukey/Bonferroni post-hoc test. Significant differences are indicated by *P<0.05 compared with untreated samples. (e) Immunostaining of control, DAPT- or IL-13-treated cultures at 72 hpi with antibodies against MUC5AC (goblet cell marker), FOXJ1 (ciliated cell marker) and SARS-CoV-2 N protein in combination with DAPI for nuclear staining. Immunofluorescence images shown are representative merged z-stack images for results of 3 independent experiments with 400 x original magnification.

Origin and culture duration of human airway epithelial cells affect SARS-CoV-2 infection

Next, we wanted to investigate how differentiation time and anatomical origin of the epithelial cultures affected SARS-CoV-2 infection biology. To this end, we employed cells isolated from bronchial or tracheal tissue and allowed ALI-PBEC and ALI-PTEC to differentiate for 3, 4 or 5 weeks, after which they were infected with 30,000 PFU of SARS-CoV-2. Viral load was analysed at 72 hpi. In both ALI-PBEC and ALI-PTEC, an increase in intra- and extracellular viral RNA as well as infectious virus particles was observed with longer differentiation time, with the highest viral load observed in cultures differentiated for 5 weeks after start of ALI (**Figure 3a-3c**). A gradual 1-2 log increase in SARS-CoV-2 progeny production was observed when cultures had been differentiated up to 5 weeks when compared to 3 weeks of differentiation (**Figure S3a**). Immunofluorescence staining of these cultures for the viral nucleocapsid protein also demonstrated an increase in the number of infected cells with increasing culture duration (**Figure 3c**). Significantly higher viral load was observed in ALI-PBEC compared to ALI-PTEC, with an average 10-fold difference in extracellular SARS-CoV-2 RNA copies (**Figure 3a-3b**) and infectious progeny (**Figure 3c**), in particular in 5-week differentiated cultures. In conclusion, our results show that both the anatomical origin of the epithelial cells and the culture duration had a profound effect on the susceptibility of airway epithelial cells to SARS-CoV-2 infection.

Time of culturing affects the proportion of cell types related to mucociliary clearance

Since we found increased viral infection upon prolonged differentiation time and additionally we observed that SARS-CoV-2 infection targets mostly ciliated cells, goblet cells and transient secretory cells (which we also confirmed for ALI-PTEC (**Figure S3c**)), we hypothesized that the numbers of these target cells changed over time of differentiation. We compared cellular composition between 3, 4 and 5 week-differentiated cultures and found that these cultures at all time points expressed markers related to all dominant epithelial cell types (ciliated, goblet, club and basal cells) in ALI-PBEC and PTEC (**Figure S3b**). However, there were clear differences in the proportions of goblet and ciliated cells over time of differentiation (**Figure 3d**). Using FOXJ1 and acetylated α-tubulin as markers for ciliated cells, we observed that the percentage of $FOXJ1^+$ cells was significantly higher in ALI-PBEC after 5-week culture compared to 3-week cultures. Also the percentage of ciliated cells was significantly higher in ALI-PBEC than in ALI-PTEC at all culture durations (**Figure 3e**). The change in the percentage of $MUC5AC^+$ goblet cells was not significant over time in ALI-PBEC and ALI-PTEC (**Figure 3e**). Additionally, the number of transient secretory cells was higher in ALI-PBEC than in ALI-PTEC (**Figure 3e**). Furthermore, mRNA levels of *FOXJ1* were significantly increased in 4 week ALI-PBEC compared to 3 week cultures, however they did not further increase in 5 week cultures (**Figure S3d**). In addition, *FOXJ1* mRNA was higher in 4/5-week ALI-PBEC cultures compared to 4/5-week PTEC cultures (**Figure S3d**). *MUC5AC* mRNA levels were higher at week 5 in ALI-PTEC cultures compared to week 3, and also higher than in week 5 ALI-PBEC (**Figure S3d**). In contrast, there was no significant difference in the expression of *SCGB1A1* (club cell marker) and *TP63* (basal cell marker) (**Figure S3d**). These results suggest that despite the early presence of transcripts which are specific for certain cell types, differentiation of certain cell types (which also requires expression at the protein level) continues for several weeks in cultures at ALI. Altogether, we found differences in the percentage of ciliated cells between PTEC and PBEC and between cultures that differed in their incubation time at ALI, which was in line with differences in viral load.

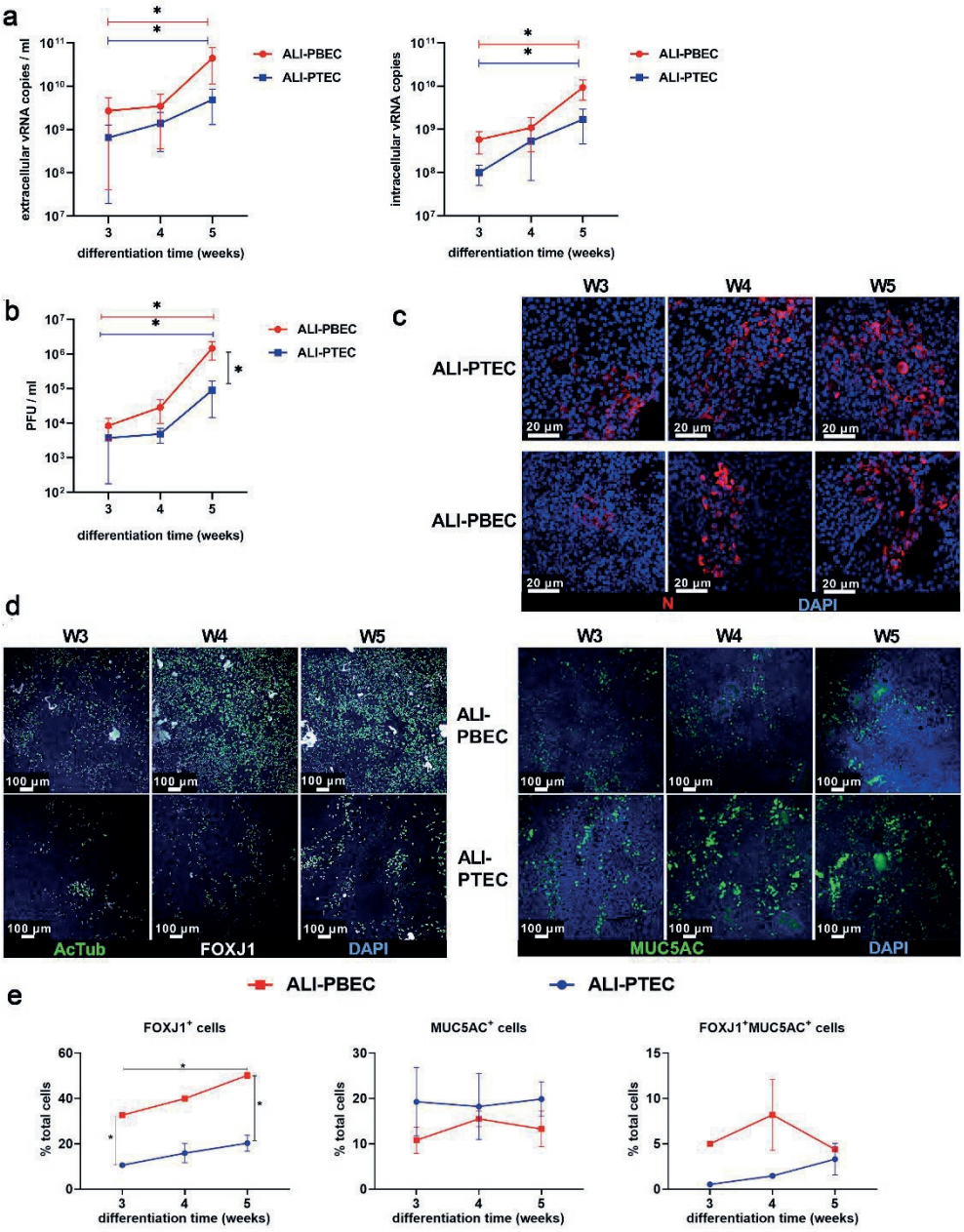

Figure 3: Effect of culture duration on SARS-CoV-2 infection in PTEC and PBEC. ALI-PBEC/ALI-PTEC (mix of 5 donors) cultured for 3-5 weeks were infected with SARS-CoV-2 (30,000 PFU per insert). (a) Extracellular viral RNA copies in the apical wash or intracellular copies were measured by RT-qPCR. (b) Viral infectious progeny was quantified by plaque assay in Vero E6 cells. Mean values ± SEM from 3 independent experiments using 3 different donor mixes are shown. Statistical analysis was conducted using two-way ANOVA with a Tukey/Bonferroni post-

hoc test. Significant differences are indicated by *P<0.05. (c) Cells were stained for immunofluorescence microscopy with rabbit polyclonal anti-SARS-CoV-2 N protein antibody (JUC3) and DAPI for nuclear staining. Images shown are representative merged z-stack images for results obtained with ALI-PBEC and ALI-PTEC from the same 3 independent experiments shown in A-B at 400 x original magnification. (d) Immunofluorescence staining of 3, 4, 5 week cultures using antibodies against acetylated α-tubulin and FOXJ1 (ciliated cell markers) or MUC5AC (goblet cell marker) in combination with DAPI for nuclear staining. Images shown are representative merged z-stack images for results of 3 independent experiments with 100x original magnification. (e) Quantification of $FOXJ^+$, $MUC5AC^+$ cells and $FOXJ1^+MUC5AC^+$ cells was done by Image J software.

Changes in gene expression associated with SARS-CoV-2 target cells

To further explore the gradual increase in susceptibility to SARS-CoV-2 infection with longer culture time, we compared the expression profiles of 3-week and 5-week uninfected differentiated cultures by bulk RNA-Seq and applied cellular deconvolution. We identified 169 differentially expressed genes, of which expression of 49 genes was upregulated while expression of 120 genes was downregulated in ALI-PBEC at 5 vs 3 weeks (Figure 4a and **Table S1**). In ALI-PTEC, the expression of 32 genes increased, and 26 genes showed decreased expression in 5-week cultures compared to 3-week cultures (**Figure 4b** and **Table S1**). Gene set enrichment analysis was conducted to identify the top differentially upregulated and downregulated gene sets in ALI-PBEC between week 5 and week 3 (**Table 1**). A striking difference in ALI-PBEC between week 5 and week 3 was observed for the gene sets related to markers of ciliated and basal cells. Cellular deconvolution analysis further showed that the relative proportion of ciliated cells was increased in 5-week ALI-PBEC cultures and the same trend was also found for ALI-PTEC (**Figure 4c** and **4d**). Altogether, RNA-Seq analysis did not reveal additional changes in cell types between the 3 and 5 week culture duration.

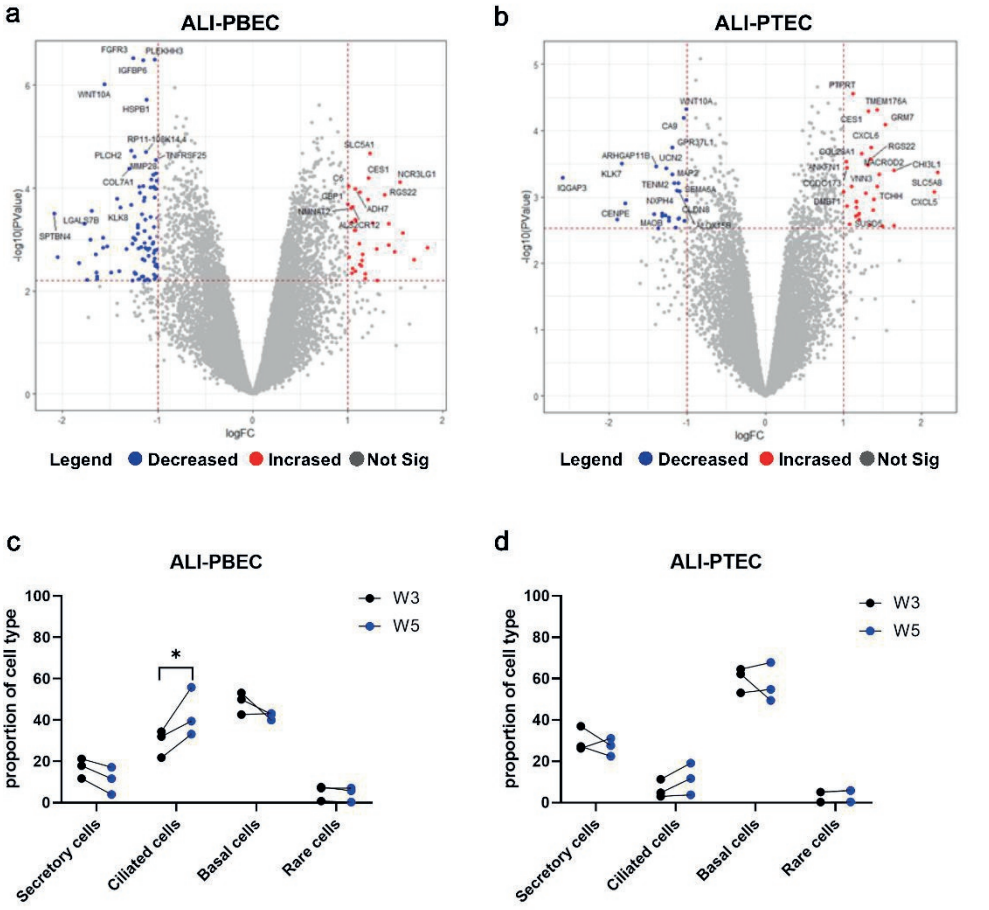

Figure 4: Transcriptional responses comparing 3 and 5 weeks-differentiated primary bronchial and tracheal cells using RNA-Seq analysis. PBEC and PTEC were cultured at ALI for 3 weeks or 5 weeks. RNA was isolated from these samples and used for RNA-Seq analysis. (a-b) Volcano plots depicting changes in the gene expression profiles of 5-week cultures compared to 3-week cultures from ALI-PBEC or ALI-PTEC. The DEGs were considered significant when they had a Benjamini Hochberg p value<0.1 and a fold change>|2. Genes depicted in red are significantly upregulated while genes depicted in blue are significantly downregulated in 5-week cultures compared to 3-week cultures in ALI-PBEC (a) or ALI-PTEC (b). (c-d) The relative proportion of different cell types for each donor mix in ALI-PBEC (c) cultures and ALI-PTEC (d) cultures as determined by cellular deconvolution of the transcriptomic datasets.

Table 1: Top 10 gene sets of the differentially expressed genes analyzed using gene set enrichment analysis (GSEA). P value was calculated from the hypergeometric distribution for (k-1, K, N - K, n) where k is the number of genes in the intersection of the query set with a set from MSigDB; K is the number of genes in the set from MSigDB; N is the total number of gene universe (all known human gene symbols); n is the number of genes in the query set. FDR q-value means the false discovery rate analog of hypergeometric p-value after correction for multiple hypothesis testing according to Benjamini and Hochberg. The gene sets related to cellular composition of lung are highlighted in bold.

Direction	Gene Set Name	# Genes in Gene Set (K)	Description	# Genes in Overlap (k)	k/K	p-value	FDR q-value
Upregulated	MURARO_PANCREAS_DUCTAL_CELL	1276		12	0.0094	9.25E-9	1.79E-4
Upregulated	GOBP_DEFENSE_RESPONSE	1739	Reactions, triggered in response to the presence of a foreign body or the occurrence of an injury, which result in restriction of damage to the organism attacked or prevention/recovery from the infection caused by the attack. [GOC:go_curators]	12	0.0069	2.7E-7	2.3E-3
Upregulated	WP_PROXIMAL_TUBULE_TRANSPORT	58	Proximal tubule transport	4	0.0690	5.25E-7	2.3E-3
Upregulated	WP_NRF2_PATHWAY	145	NRF2 pathway	5	0.0345	5.77E-7	2.3E-3
Upregulated	DESCARTES_FETAL_INTESTINE_INTESTINAL_EPITHELIAL_CELLS	276	descartes DE_gene_by_organ.csv, fold.change>5, qval<0.05, pval<0.05	6	0.0217	5.94E-7	2.3E-3
Upregulated	REACTOME_G_ALPHA_I_SIGNALLING_EVENTS	314	G alpha (i) signalling events	6	0.0191	1.26E-6	3.46E-3
Upregulated	GOMF_SOLUTE_SODIUM_SYMPORTER_ACTIVITY	72	Enables the transfer of a solute or solutes from one side of a membrane to the other according to the reaction: solute(out) + Na+(out) = solute(in) + Na+(in). [GOC:ai]	4	0.0556	1.26E-6	3.46E-3
Upregulated	WP_NUCLEAR_RECEPTORS_METAPATHWAY	321	Nuclear receptors meta-pathway	6	0.0187	1.43E-6	3.46E-3
Upregulated	**TRAVAGLINI_LUNG_CILIATED_CELL**	**1094**		**9**	**0.0082**	**2.59E-6**	**5.57E-3**
Upregulated	TRAVAGLINI_LUNG_MACROPHAGE_CELL	201		5	0.0249	2.88E-6	5.58E-3
Downregulated	GOCC_SUPRAMOLECULAR_COMPLEX	1329	A cellular component that consists of an indeterminate number of proteins or macromolecular complexes, organized into a regular, higher-order structure such as a polymer, sheet, network or a fiber. [GOC:dos]	18	0.0135	9.81E-9	8.53E-5
Downregulated	**TRAVAGLINI_LUNG_PROLIFERATING_BASAL_CELL**	**891**		**15**	**0.0168**	**1.12E-8**	**8.53E-5**
Downregulated	HAY_BONE_MARROW_STROMAL	767		14	0.0183	1.32E-8	8.53E-5

Downregulated	TRAVAGLINI_ LUNG_BASAL_CELL	188		8	0.0426	3.6E-8	1.61E-4
Downregulated	GOCC_SUPRAMOLECULAR_POLYMER	996	A polymeric supramolecular structure. [GOC:dos]	15	0.0151	4.84E-8	1.61E-4
Downregulated	ZHONG_PFC_C2_ UNKNOWN_NPC	76		6	0.0789	5.04E-8	1.61E-4
Downregulated	HALLMARK_KRAS_ SIGNALING_DN	200	Genes down-regulated by KRAS activation.	8	0.0400	5.81E-8	1.61E-4
Downregulated	NABA_ MATRISOME	1026	Ensemble of genes encoding extracellular matrix and extracellular matrix-associated proteins	15	0.0146	7.1E-8	1.72E-4
Downregulated	MANNO_MIDBRAIN_NEUROTYPES_ HNPROG	229	Cell types are named using anatomical and functional mnemonics prefixed by 'm' or'h' to indicate mouse and human respectively: OMTN, oculomotor and trochlear nucleus; Sert, serotonergic; NbM, medial neuroblast; NbDA, neuroblast dopaminergic; DA0-2, dopaminergic neurons; RN, red nucleus; Gaba1-2, GABAergic neurons; mNbL1-2, lateral neuroblasts; NbML1-5, mediolateral neuroblasts; NProg, neuronal progenitor; Prog, progenitor medial floorplate (FPM), lateral floorplate (FPL), midline (M), basal plate (BP); Rgl1-3, radial glia-like cells; Mgl, microglia; Endo, endothelial cells; Peric, pericytes; Epend, ependymal; OPC, oligodendrocyte precursor cells.	8	0.0349	1.64E-7	3.45E-4
Downregulated	FAN_EMBRYONIC_ CTX_MICROGLIA_1	155		7	0.0452	1.78E-7	3.45E-4

Cell culture duration alters expression of SARS-CoV-2 entry factors

The expression of host proteins that have been linked to entry of SARS-CoV-2 varies between the different airway epithelial cell types (229). Therefore, we investigated whether the observed increase in susceptibility to SARS-CoV-2 with increased differentiation time and the effect of the anatomical origin, was related to the expression of the main receptor ACE2, or other factors involved in entry. We compared the mRNA levels of different viral entry factors between the single-donor cultures that displayed the highest and lowest viral load (**Figure 1a, Figure 5a**). Interestingly, the culture with the highest viral load expressed higher mRNA levels of *CTSL* and *TMPRSS2* at baseline, while other factors did not differ.

Furthermore, we assessed the expression of cell-entry factors in cultures of varying differentiation time using our RNA-Seq dataset (**Figure 5b**). In both ALI-PBEC and ALI-PTEC cultures, there was a significant increase in expression of *TMPRSS2* in 5-week cultures compared to 3-week cultures. In addition, expression of *CTSL* was significantly increased while expression of *CD147* was decreased at 5 weeks compared to 3 weeks in ALI-PBEC. However, expression of *NRP1* was reduced at 5 weeks compared to 3 weeks in ALI-PTEC, and expression of *ACE2*, *FURIN* and *NRP1* was lower in 3-week ALI-PBEC compared to 3-week ALI-PTEC (**Figure 5b**). We compared the expression of these genes by RT-qPCR in 3- and 5-week cultures, and also included 4-week cultures (**Figure S4a**). With longer culture duration, in both ALI-PBEC and ALI-PTEC, gene expression of *CTSL* and *TMPRSS2* indeed increased over time and a significant increase was found in expression of *TMPRSS2* in 4-week ALI-PBEC compared to 3-week cultures. Gene expression of *ACE2* and *GRP78* did not change with culture duration. A significant increase in expression of *CD147* was observed in 4-week ALI-PBEC compared to 3-week cultures (**Figure S4a**). Treatment with DAPT or IL-13 did not affect expression of SARS-CoV-2 entry factors (**Figure S4b**). These findings indicated that changes in expression of *CTSL* and *TMPRSS2* could (in part) be responsible for the observed differences in susceptibility to SARS-CoV-2 infection between 3-, 4- and 5-week differentiated cultures.

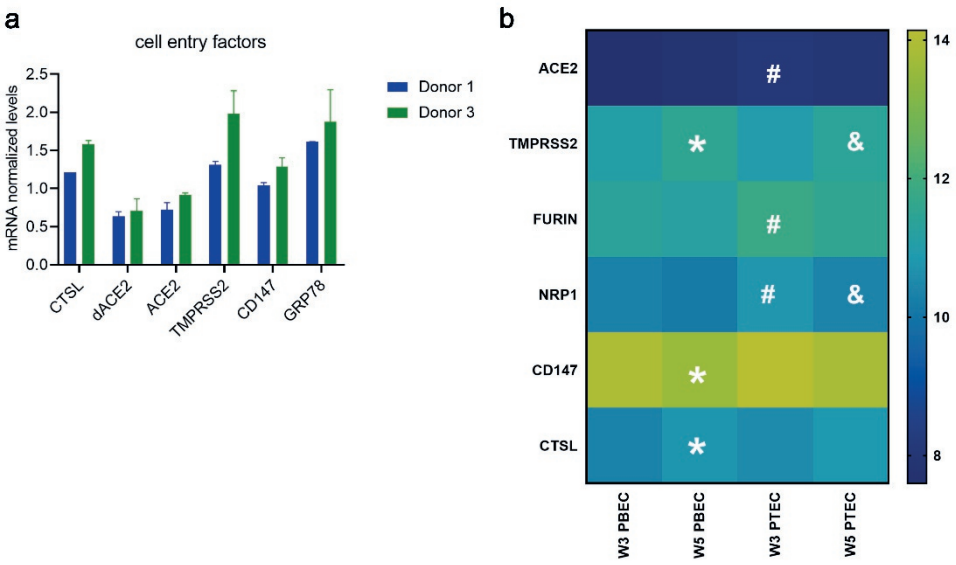

Figure 5: Effect of donor variation and culture duration on expression of SARS-CoV-2 cell-entry factors. (a) RT-qPCR analysis of gene expression of viral cell-entry factors in two single donor cultures at 5 weeks. Data are mean values ± SEM. n=2 duplicated wells per donor. (b) Heatmap of transcriptional changes (RNA-Seq data) of SARS-CoV-2 cell-entry factors in 3-week and 5-week PBEC and PTEC. Differences were assessed by a two-way ANOVA

with Tukey's test and the significant difference were considered at $P < 0.05$. *= 5-week ALI-PBEC vs 3-week ALI-PBEC; &=5-week ALI-PTEC vs 3-week ALI-PTEC; #=3-week ALI-PTEC vs 3-week ALI-PBEC.

Cell culture duration does not affect SARS-CoV-2-induced antiviral responses

Antiviral responses in the epithelium are critical for protection against viral infections. Therefore, we investigated whether antiviral responses changed depending on the ALI culture duration, and whether this could provide an additional explanation of the observed increased susceptibility to infection with longer culture times. In ALI-PTEC, SARS-CoV-2-induced mRNA levels of both *IFNB1* and *IFNL1* increased significantly with culture duration. When cultures were infected at week 3 or 4 there was little *IFNB1* or *IFNL1* mRNA produced, while expression of these genes was strongly upregulated by SARS-CoV-2 infection in 5 week old cultures (**Figure S5a** and **S5b**). Gene expression analysis of *IFNB1* and *IFNL1* showed a similar increasing trend in ALI-PBEC upon infection (**Figure S5c** and **S5d**). When 5-week PBEC were (long-term) treated with DAPT, we observed lower SARS-CoV-2-induced antiviral responses than in untreated and IL-13-treated cultures (**Figure S5e** and **5f**). All these findings correlate with the observed differences in the number of infected cells and viral load resulting from culture duration and DAPT and IL-13 treatment (**Figure 2**). This suggests that antiviral responses were not affected by differentiation time or long-term DAPT/IL-13 treatment, but rather differed as a direct consequence of differences in the level of infection.

Discussion

Here we investigated the influence of cellular composition and differentiation of human primary airway epithelial cell cultures on SARS-CoV-2 infection biology. Our key finding is that changes in cell types related to mucociliary clearance, i.e. ciliated and goblet cells, influence SARS-CoV-2 infection of human primary airway epithelial cells. Specifically, a higher percentage of ciliated cells appears to be the main contributing factor to a higher level of infection. This is likely a consequence of their higher susceptibility to infection in comparison to the other cell-types, and possibly their contribution to spreading of virus across the epithelial surface of the culture. Nevertheless, our data also suggest that the presence of mucus and/or goblet cells is important, since a reduction in goblet cells reduced viral load, even in cultures with a higher percentage of ciliated cells. Finally, we provide experimental evidence for infection of transient secretory cells by SARS-CoV-2.

With regard to differentiation time, there is no golden standard protocol for ALI-primary airway epithelial cell cultures to obtain cultures that best resemble the human epithelial

cellular composition. Literature reports that differentiation times anywhere between 2 and 6 weeks after start of air-liquid interface culture are needed to have all key cell-types present in culture (71, 226, 240).

In line with a recent study investigating SARS-CoV-2 infection using primary airway epithelial cells(226), and based on our own study comparing 3-5 week old cultures, we decided to use 5 weeks differentiated ALI-PBEC cultures. We found a reproducible increase in viral titers over time post infection. In addition, cultures of well-differentiated airway epithelial cells adequately model *in vivo* host antiviral responses (137, 241), which we could confirm also for SARS-CoV-2 infection by detecting increased mRNA levels of *IL-6* and *CXCL8*. In contrast, downregulated expression of *IL-6* and *CXCL8* was reported in the human bronchial epithelial cell line 16HBE (242).

We confirmed that both ciliated and goblet cells were infected by SARS-CoV-2 in our ALI-cultures, whereas no infected club and basal cells were detected (data not shown). This is consistent with results from recent studies looking into the cellular tropism of SARS-CoV-2 showing infection of multiple epithelial cell types, among them ciliated cells, goblet cells and club cells of the airway epithelium, and type 2 alveolar epithelial cells (68, 71, 226, 243). Additionally, we also observed cells co-expressing markers of ciliated cells (FOXJ1) and goblet cells (MUC5AC) in our cultures. This specific cell population, which was recently reported by e.g. Garcia *et al.* (244) and by Vieira Braga et al (245), is suggested to represent a transitional state between goblet and ciliated cells, and was recently labelled as transient secretory cells (231). Based on their relatively high co-expression of ACE2 and TMPRSS2, Lukassen et al. (231) suggested that these transient secretory cells may be particularly vulnerable to SARS-CoV-2 infection. Whereas we showed for the first time that SARS-CoV-2 was also able to infect these cells, it remains unknown if the low percentage of these cells in our culture model significantly contributed to the overall level of infection. Considering the role in mucociliary clearance of ciliated, goblet and potentially transient secretory cells, we conclude that cells involved in mucociliary clearance are predominantly infected by SARS-CoV-2.

To investigate the role of cellular composition in susceptibility to viral infection, we skewed cell differentiation with the Notch signalling inhibitor DAPT (238), which resulted in cultures that constituted a high number of ciliated cells but lacked goblet cells and transient secretory cells. Surprisingly the viral load in these cultures was reduced compared to untreated cultures. A possible explanation would be that ciliated cells become infected by the virus, and mucus produced by goblet cells helps spread the infection after release, which would be consistent with previous findings that SARS-CoV-2 infects ciliated cells with attached mucus (246). Conversely, the modulation with IL-13, (slightly) increased viral loads compared to control and DAPT-treated cultures, which is in line with the suggestion from

other studies that patients with allergic asthma, a disease associated with IL-13-induced changes in epithelial cell composition, may be somewhat more susceptible to SARS-CoV-2 infection (247). Others have observed that treatment with IL-13 reduced viral RNA copies in ALI-cultured airway epithelial cells (248, 249). There is no clear explanation for this discrepancy, although the reduced levels of *ACE2* after IL-13 treatment that were found in these studies might have been responsible for the reduced infection levels. However, in our studies ACE2 expression was not affected by IL-13 treatment. Furthermore, we used a much lower MOI (0.03 versus 0.5), and therefore even if IL-13 reduces the number of the main target cells (e.g. ciliated cells) this is not expected to have much effect in our setup, because the amount of susceptible cells will likely not be limiting due to the low MOI. Collectively, our observations indicate that DAPT- and IL-13-mediated modulation of epithelial cell differentiation does not provide a simple link between differences in epithelial cell composition and susceptibility to SARS-CoV-2 infection. A combination of factors appears to play a role. For example, mucus secretion by goblet cells (250), when excessive, could hinder clearance of the virus in the epithelium. We therefore used additional approaches to study the contributing effect of cellular composition to SARS-CoV-2 infection. We could demonstrate that changes in cellular composition either linked to anatomical origin, donor or culture time, influenced SARS-CoV-2 infection. The shared outcome was that for each variable the number of target cells correlated to the viral load, suggesting that the percentage of ciliated cells is a strong contributing factor to the SARS-CoV-2 infection rate. Considering that expression of viral entry factors varies between different cell types, we furthermore investigated their expression in cells from different donors, the effect of culture duration, and the impact of treatment with DAPT and IL-13. According to literature, all main cell types express *TMPRSS2,* and highest expression is found in transient secretory cells (231). *CTSL* gene expression was reported to be higher in ciliated cells compared to other epithelial cell types (251). When we compared two single donors, cell cultures isolated from one donor expressed more *CTSL* and *TMPRSS2,* which was in line with the observed higher viral replication and higher abundance of ciliated cells in this donor. In our study, an increased expression of *CTSL* as well as *TMPRSS2* was also found with prolonged culture duration. Thus, the difference in *CTSL* expression could link to changes in the ciliated cell number, which supports the role of ciliated cells in viral replication. Furthermore in line with this, CTSL levels were recently found to be positively correlated with severity of disease in COVID-19 patients, pointing to its role in enhancement of infection (252). Other studies evaluated the role of CTSL and TMPRSS2 in SARS-CoV-2 infection by using E64d (an inhibitor of cysteine proteases, including CTSL) and camostat mesylate (an inhibitor of serine proteases, including TMPRSS2) (228, 253). It was shown that both E64d and camostat

mesylate inhibited infection by Wuhan, Delta and Omicron isolates, confirming the role of CTSL and TMPRSS2 in viral entry.

We excluded possible effects of changes in antiviral responses on the gradual increase in viral infection with the prolonged culture duration, since we did not observe lower expression of type I and III IFNs over culture time at ALI, but rather found a correlation with the level of viral replication.

Our study demonstrates that the use of mixed donor cultures is an efficient way to recapitulate natural variability between donors while saving on resources (cells, culture plastics and media) that can be in high demand/short supply during pandemics. The level of donor-to-donor variation was also represented in inter-experimental variation when using the same donor mix. Inevitably, our study has some limitations. First, it needs to be noted that the comparison between PBEC and PTEC in this study should be interpreted with caution, because PBEC were derived from tumor-free resected bronchial tissue from (ex-) smoking patients with lung cancer, and PTEC were from donor lungs without lung disease. Second, the fact that we used an early pandemic SARS-CoV-2 strain in our studies could be considered a limitation, but this variant is still widely used as model in (fundamental) studies on virus replication and antivirals. Studying this virus is still important to increase our preparedness for future outbreaks of highly pathogenic zoonotic coronaviruses. Several other studies have already compared the replication of different viruses, including recent omicron variants in human airway epithelial cell cultures (75, 140, 253). It would be interesting to investigate if variants like alpha or delta, which have been reported to have a replicative advantage in human airway epithelial cell cultures, are likewise impacted by the changes in differentiated cultures that we observed in this study. Finally, we used cultures containing only epithelial cells. Adding immune cells to the culture system could offer interesting possibilities for future studies to investigate their impact on host responses during infection.

Overall, in this study we have established that epithelial cell types related to mucociliary clearance (i.e. ciliated, goblet cells and transient secretory cells) seem pivotal for SARS-CoV-2 infection and spread of the infection over the epithelial tissue. This study underlines the importance of assessing these cell types and the role of mucus when studying how SARS-CoV-2 infection biology is affected in patients with chronic lung disease, such as those with chronic type 2 inflammation in asthma or in COPD, where epithelial remodelling likely has shifted these cell-type ratios.

Materials and Methods

Cell culture

PBEC were isolated from tumor-free resected bronchial tissue that was obtained from patients undergoing resection surgery for lung cancer at the Leiden University Medical Center (Leiden, the Netherlands). Patients from which this PBEC were derived were enrolled in the biobank via a no-objection system for coded anonymous further use of such tissue (www.coreon.org). However, since 1-9-2022, patients have been enrolled in the biobank using active informed consent in accordance with local regulations from the LUMC biobank with approval by the institutional medical ethical committee (B20.042/Ab/ab and B20.042/Kb/kb). PTEC were isolated from residual tracheal and main stem bronchial tissue from lung transplant donors post-mortem at the University Medical Center Essen (Essen, Germany). Use of such donor tissue for research was approved by the ethical committee of the Medical faculty of the University Duisburg-Essen (ID: 19-8717-BO). (254).

To achieve mucociliary differentiation, PBEC and PTEC were cultured at the ALI as previously described (237). Briefly, epithelial cell cultures from individual donors or mixed donors were seeded onto 12-insert Transwell membranes (Corning Costar, Cambridge, MA, USA), which were coated with PBS supplemented with 5 µg/ml human fibronectin (Promocell, Heidelberg, Germany), 30 µg/ml PureCol (Advanced BioMatrix, CA, USA) and 10 µg/ml bovine serum albumin (Fraction V; Thermo Fisher Scientific, Carlsbad, CA, USA), in a 1:1 mixture of Bronchial Epithelial Cell Medium-basal (BEpiCM-b; ScienCell, Sanbio) and Dulbecco's modified Eagle's medium (DMEM) (Stemcell Technologies, Köln, Germany), further referred to as B/D medium. This B/D medium contains 12.5 mM HEPES, bronchial epithelial cell growth supplement, 100 U/ml penicillin, 100 ug/ml streptomycin (all from ScienCell), 2 mM glutaMAX (Thermo Fisher Scientific). B/D medium was supplemented during submerged culture with 1 nM EC23 (light-stable retinoic acid receptor agonist; Tocris, Abingdon, UK). For individual donors, the seeding intensity was 40,000 cells/12-insert and for mixed donors approximately 150,000 cells (30,000 cells/donor when mixing cells from 5 donors and 40,000 cells/donor when using 4 donors). For the donor mixes, the higher seeding density compared to individual cultures resulted in near-confluency to avoid selective advantage of possible faster-proliferating cells of specific donors.After confluency was reached, the apical medium was removed and cells were cultured at the ALI in B/D medium with 50 nM EC23 for 3-5 weeks; during this period, medium was refreshed and the apical side was washed three times a week with warm PBS to remove excess mucus.

To shift cell differentiation towards an increased number of goblet or ciliated cells, ALI- PBEC were incubated in BD medium supplemented with 50 nM EC23, and either 1 ng/ml IL-13 (Peprotech) or 5 µM DAPT (γ-secretase inhibitor, TOCRIS) from day 22 to day 35 culture

time. To assess the direct effect of DAPT, we treated cells with DAPT either starting 24 h before (and during) infection (a time period considered insufficient to cause a shift in epithelial differentiation) or directly after infection.
Vero E6 cells (master stock MM-3 from dept. of Medical Microbiology collection, characterized by full genome sequencing) were maintained in Dulbecco's modified Eagle's medium with 4.5 g/l glucose with L-glutamine (DMEM; Lonza), supplemented with 8% foetal calf serum (FBS; CapriCorn Scientific) and 100 U/ml of penicillin/streptomycin (Sigma-Aldrich). All cell cultures were maintained at 37°C. Infections for plaque assays in Vero E6 cells were performed in Eagle's minimal essential medium with 25 mM HEPES (EMEM; Lonza) supplemented with 2% FCS, 2 mM L-glutamine (Sigma-Aldrich), and 100 U/ml of penicillin/streptomycin (Sigma-Aldrich) .

SARS-CoV-2 virus

The clinical isolate SARS-CoV-2/Leiden-0002 was isolated from a nasopharyngeal sample collected at the LUMC (GenBank accession nr. MT510999). The virus was passaged twice in Vero E6 cells to obtain the virus stock used for infection. Virus titers were determined by plaque assay as described before (255). All experiments with infectious SARS-CoV-2 were performed at the Leiden University Medical Center biosafety level 3 facilities.

SARS-CoV-2 infection of ALI-PBEC

Prior to infection, the mucus was removed by washing the apical surface of the ALI cultures with 200 µl PBS and aspirating it after a 10-min incubation at 37°C. Basal medium was changed every two days. Cells were infected with 200 µl of inoculum prepared in PBS, containing 30,000 PFU of SARS-CoV-2, per insert for 2 h at 37°C on a rocking platform (estimated MOI of 0.03). PBS was used as solvent control and in mock-infected cells as inoculum. After removal of the inoculum, the apical side was washed three times with PBS and cells were incubated at 37°C. Viral progeny was harvested from the apical side at 24, 48 and 72 hpi as described in the next section.
Cells were infected after 3 to 5 weeks of differentiation as indicated. For cells under DAPT or IL-13 treatment, the medium was supplemented with 1 ng/ml IL-13 or 5 µM DAPT after 3 weeks of differentiation, and after 5-week culture time in total (2 weeks of treatment), PBEC were infected. After infection, the basal medium was replaced by fresh B/D medium also supplemented with IL-13 or DAPT.

RNA isolation, quantitative RT-PCR/real-time PCR (RT-qPCR) and plaque assay analysis

Apical washes were harvested following a 10-min incubation at 37°C with 200 µl PBS. RNA was isolated from half the volume of apical washes (100 µl) after addition of 800 ul of TriPure Isolation Reagent (Sigma-Aldrich). Tripure reagent was spiked with Equine arteritis virus (EAV) to control for variation in RNA extraction efficiency and possible inhibitors of RT-qPCR. Intracellular RNA was isolated by adding 500 ul of TriPure reagent directly to cells on the insert. Samples were stored at -20°C until RNA was isolated using the Direct-zol™ -96 RNA plate isolation (Zymo), 5PRIME Phase Lock Gel extraction (Quantabio) or Maxwell® 16 simply RNA tissue kit (Promega, the Netherlands). The Phosphoglycerate kinase 1 (*PGK-1*) was used as a reference gene for normalization when intracellular RNA was analysed. Primers and probes for EAV and *PGK-1* (Sigma-Aldrich) and the normalization procedure were performed as described before(255). Viral RNA was quantified by internally controlled multiplex RT-qPCR using the TaqMan™ Fast Virus 1-Step Master Mix (Thermo Fisher Scientific) as described previously (256), but with modifications as listed in **Table 2**. A standard curve generated by RT-qPCR on 10-fold serial dilutions of a T7 RNA polymerase-generated *in vitro* transcript containing the target sequences was used for absolute quantification of RNA copy numbers.

For analysis of the transcriptional response of epithelial cells to infection, RNA was reverse-transcribed and cDNA was amplified by real-time qPCR (Bio-Rad, Veenendaal, the Netherlands) using specific primers. Relative normalized gene expression compared to reference genes Ribosomal Protein L13a (RPL13A) and ATP synthase, H^+ transporting, mitochondrial F1 complex, beta polypeptide (ATP5B) were calculated according to the standard curve method. Reference genes were selected out of 8 candidate reference genes using the "Genorm" software (Genorm; Primer Design, Southampton, UK). RT-qPCR was performed on a CFX384 Touch™ Real-Time PCR Detection System (Bio-Rad) using a program consisting of 5 min at 50°C and 20 s at 95°C (or 3 min at 95°C when cDNA was used), followed by 45 cycles of 5 s at 95°C and 30 s at 60°C or 63°C (depending on primers). Primer pairs are listed in **Table 2**.

For quantification of the number of infectious virus particles, the apical wash was serially diluted and infectious titers were determined by plaque assay on Vero E6 as described previously (255).

Table 2: Primer sequences

Gene	Forward primer (5'-3')	Reverse primer (5'-3')
E	ACAGGTACGTTAATAGTTAATAGCGT	ATATTGCAGCAGTACGCACACA
E probe	TexRed-ACACTAGCCATCCTTACTGCGCTTCG-BHQ1	
RdRp	GTGARATGGTCATGTGTGGCGG	CARATGTTAAASACACTATTAGCATA

RdRp probe	FAM-CAGGTGGAACCTCATCAGGAGATGC-BHQ1	
MUC5AC	CCTTCGACGGACAGAGCTAC	TCTCGGTGACAACACGAAAG
FOXJ1	GGAGGGGACGTAAATCCCTA	TTGGTCCCAGTAGTTCCAGC
SCGB1A1	ACATGAGGGAGGCAGGGGCTC	ACTCAAAGCATGGCAGCGGCA
TP63	CCACCTGGACGTATTCCACTG	TCGAATCAAATGACTAGGAGGGG
IFNL1	GGACGCCTTGGAAGAGTCACT	AGAAGCCTCAGGTCCCAATTC
IFNB1	ATGACCAACAAGTGTCTCCTCC	GGAATCCAAGCAAGTTGTAGCTC
CXCL8	CTGGACCCCAAGGAAAAC	TGGCAACCCTACAACAGAC
IL6	CAGAGCTGTGCAGATGAGTAC A	GATGAGTTGTCATGTCCTGCA
ACE2	CGTCTGAATGACAACAGCCTAGA	AATGCCAACCACTATCACTCCC
TMPRSS2	AATCGGTGTGTTCGCCTCTAC	CGTAGTTCTCGTTCCAGTCGT
CD147	CAGAGTGAAGGCTGTGAAGTCG	TGCGAGGAACTCACGAAGAAC
GRP78	GGAAAGAAGGTTACCCATGC	AGAAGAGACACATCGAAGGT
ATP5B	TCACCCAGGCTGGTTCAGA	AGTGGCCAGGGTAGGCTGAT
RPL13A	AAGGTGGTGGTCGTACGCTGTG	CGGGAAGGGTTGGTGTTCATCC

Immunofluorescence staining

For analysis by immunofluorescence, ALI cultures were rinsed using PBS and cells were fixed by adding 3% (w/v) paraformaldehyde diluted in PBS into the basal and apical compartments followed by incubation at room temperature for at least 35 min. Next, inserts were washed two times with PBS and stored in PBS with 10 mM glycine at 4°C until further use. Ice-cold methanol was added for 10 min at 4°C, and PBS containing 1% (w/v) BSA, 0.3% (w/v) Triton-X-100 (PBT) was used to block non-specific binding sites and permeabilize cells for 30 min at 4°C. Membranes were excised from the insert and cut into 4 pieces that were incubated overnight at 4°C with specific antibodies at the following dilutions: rabbit anti-SARS-CoV-2 N antibody (JUC3,1:500 (167)), human anti-SARS-CoV-2 Spike antibody (P008_076 (257)), mouse anti-MUC5AC antibody (1:200; Thermo Fisher Scientific), mouse anti-acetylated α-tubulin (1/100; Sigma Aldrich) or goat anti-FOXJ1 antibody (1:200; R&D, Minneapolis, MN, USA). After washing, membranes were incubated with corresponding secondary antibodies: donkey anti-rabbit, donkey anti-mouse or donkey anti-goat Alexa-fluor antibodies (all diluted 1:200, Thermo Fisher Scientific) and 4',6-diamidino-2-phenylindole (DAPI, 1:200, Sigma-Aldrich) in the dark for 30 min at room temperature. Next, membranes were transferred to glass slides and covered with prolong gold anti-fading reagent (Thermo Fisher Scientific) and a coverslip (VWR, Amsterdam, the Netherlands). Slides were viewed using a Leica TCS SP8 confocal microscope (Leica Microsystems, Wetzlar, Germany), the Andor Dragonfly 500 spinning disk confocal (Andor Technology, Belfast, UK), or the ZEISS Axio Scan.Z1 Slide Scanner (ZEISS, Oberkochen,

Germany) at 100 x /400 x / 630 x original magnification according to experimental requirements. Positive-stained cells from three random areas of each insert membrane of each independent experiment were quantified by ImageJ.

RNA sequencing and analysis

The samples harvested from 3-week and 5-week differentiated ALI-PBEC and ALI-PTEC were used to perform RNA sequencing (RNA-Seq) at GenomeScan (Leiden, the Netherlands). Total RNA was extracted using TriPure Isolation Reagent and Maxwell® 16 simply RNA tissue kit and passed the quality control (QC) measured by the Fragment Analyzer. Then mRNA was isolated based on poly-A selection and RNA fragmentation was performed. After that, cDNA was synthesized for adapter ligation and PCR amplification. A data set of 12 samples was generated using an Illumina NovaSeq6000 sequencer and the quality for the raw data was determined with third-party (FastQC v0.11.9) and in-house (FastQA v3.1.25) QC tools. The paired-end reads were trimmed to remove possible adapter sequences using cutadapt v2.10 and mapped to the human GRCh37.75 (Homo_sapiens.GRCh37.75.dna.primary assembly.fa). Based on the mapped locations in the alignment file the frequency of how often a read was mapped on a transcript was determined with HTSeq v0.11.0. RNA-Seq analysis was performed using the R package DeSeq2 with the read counts≥10 read counts. Differential expression was conducted comparing virus infection at each time point to time matched no virus control/mock. Gene signatures were made using the Gene Set Variation Analysis (GSVA) package. The differentially expressed genes (DEGs) were generated by comparing data in 5-week cultures compared to 3-week cultures and the significant differences were considered when they had a Benjamini Hochberg p value<0.1 and a fold change>|2|. The gene sets of differentially expressed genes were further analysed by gene set enrichment analysis (GSEA) using the website www.gsea-msigdb.org as previously reported (258, 259).

Cellular deconvolution

The relative proportion of each cell type (ciliated, secretory, basal and rare cells) was predicted using cellular deconvolution analysis of bulk RNA-Seq data as previously described (260). To this end, genes were selected using AutoGeneS software on the Human Lung Cell Atlas v1.0 dataset (261) based on minimized correlation and maximized distance between clusters. After that, genes with the most stable results across cohorts were selected and used to deduce major cell type proportions. The RNA-Seq data was subsequently normalized to counts per million (CPM), and highly variable (HV) genes (N=5,000) were selected. Next, on all samples bulk deconvolution was performed using the

CIBERSORT support vector regression (SVR) method (262). The relative proportion of cell types was compared between 3-week cultures and 5-week cultures from ALI-PBEC or ALI-PTEC using paired two-way ANOVA with Tukey's test.

Statistical analysis

Statistical analysis was performed in GraphPad PRISM 9.0 (GraphPad Software Inc., La Jolla, CA). Differences were assessed by a paired one-way with Tukey's test, paired two-way ANOVA with Tukey's test or paired, two-tailed t test. Data are shown as mean values ± SEM and differences were considered significant at $P < 0.05$.

Statement of Ethics

Patients from which this PBEC were derived were enrolled in the biobank via a no-objection system for coded anonymous further use of such tissue (www.coreon.org). However, since 1-9-2022, patients have been enrolled in the biobank using active informed consent in accordance with local regulations from the LUMC biobank with approval by the institutional medical ethical committee (B20.042/Ab/ab and B20.042/Kb/kb). For the present study, cells from patients were used that were collected before 1-9-2022, and based on the regulations of the no-objection system, individual informed consent was not needed. PTEC were isolated from residual tracheal and main stem bronchial tissue from lung transplant donors post-mortem at the University Medical Center Essen (Essen, Germany). Use of such donor tissue for research was approved by the ethical committee of the Medical faculty of the University Duisburg-Essen (ID: 19-8717-BO). Written informed consent for the use of PTEC was provided by the transplant recipients of the respective lungs.

Conflict of Interest Statement

The authors have no conflicts of interest to declare.

Funding Sources

This study was supported by a COVID-19 MKMD grant from the Netherlands Organization for Health Research and Development (ZonMw) and the Dutch Society for the Replacement of Animal Testing (Stichting Proefdiervrij) (grant #114025007). C.S.-B. was supported by the Coordination for the Improvement of Higher Education Personnel (CAPES) (process no.

88881.171440/2018-01), Ministry of Education, Brazil. Part of this research was supported by the Leiden University Fund (LUF), the Bontius Foundation, and donations from the crowdfunding initiative “wake up to corona”. This study has also received funding from the European Union's Horizon 2020 research and Innovation program under grant No 10100362 (the SCORE project). Part of RNA-Seq and analysis was supported by a RSEOH-CAG Rapid Response Research Initiative and a RSEOH-CAG 2021 Extension Grant. Collection of primary human tracheal epithelial cells was supported by grants from the Deutsche Forschungsgemeinschaft (DFG) (Ta 275/7-1 and Ta 275/8-1) to C.T.

Author Contributions

Melissa Thaler, Ying Wang, Anne M. van der Does, Peter J. Bredenbeek, Pieter S. Hiemstra and Martijn J. van Hemert were involved in study design and conceptualization. Melissa Thaler, Ying Wang, Dennis K. Ninaber, Natacha S. Ogando, Clarisse Salgado-Benvindo performed experiments. Alen Faiz performed RNA-Seq analysis and cellular deconvolution. Hendrik Beckert, Christian Taube collected and isolated human tracheal epithelial cells. Melissa Thaler and Ying Wang wrote the manuscript. Anne M. van der Does, Pieter S. Hiemstra, Martijn J. van Hemert, Eric J. Snijder and Peter J. Bredenbeek revised the manuscript. The final version was critically reviewed and approved by all authors.

Data Availability Statement

The RNA-Seq data that support the findings of this study will be openly available in the repository European Genome-Phenome Archive (EGA). Until then all data are available upon reasonable request by contacting the corresponding author. All other data generated or analysed during this study are included in this article.

Supplementary Material

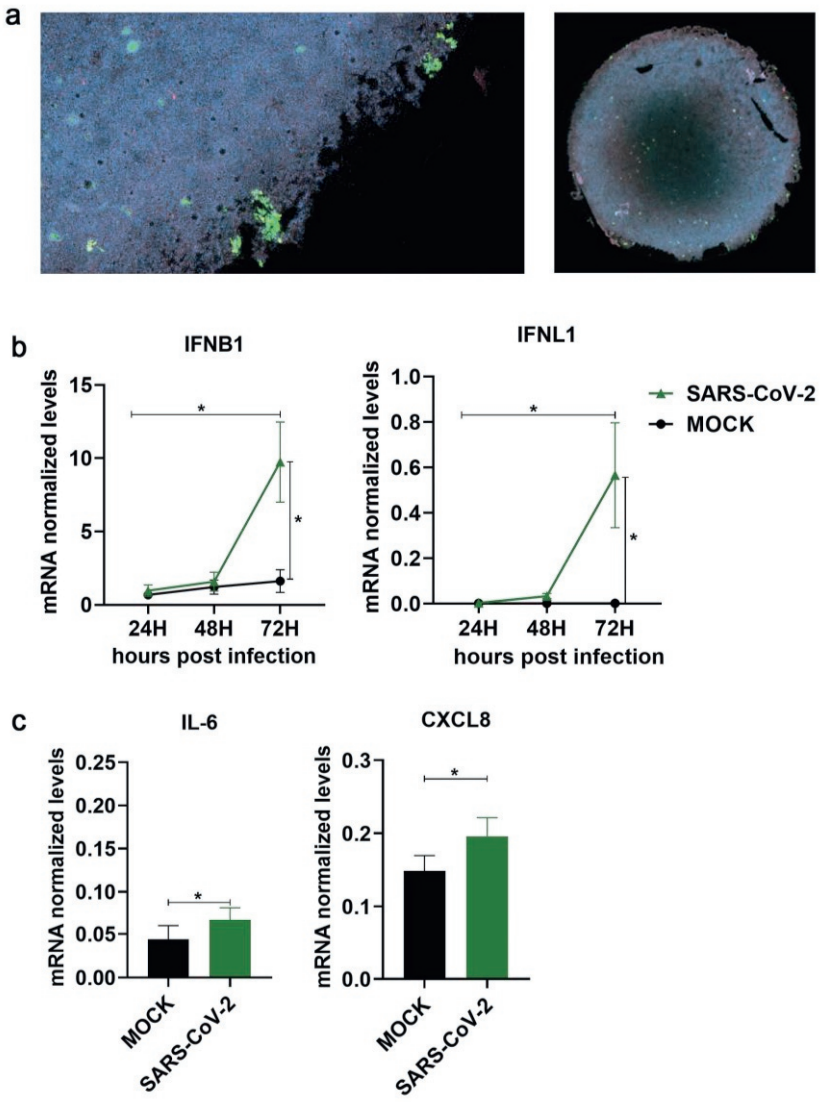

Figure S1: Infection and immune responses of a primary airway epithelial cell culture model. ALI-PBEC (mix of 5 donors) cultured for 5 weeks at ALI were infected with SARS-CoV-2 (30,000 PFU per insert) (a) Representative image of immunostaining with anti-SARS-CoV-2 spike protein antibody (green), anti-N protein antibody (JUC3; red) and DAPI (blue) for nuclear staining was captured by ZEISS slide scanner (b) Analysis of gene expression of *IFNB1*, *IFNL1* and (c) *IL6* and *CXCL8* (IL-8) normalized to two reference genes (*RPL13A/ATP5B*) in mixes of 5 donors by RT-qPCR. The graphs represent the mRNA levels at 72 hpi. Data are mean values ± SEM. n=3 independent experiments derived from the same donor mix cultured for at least 4 weeks. Statistical analysis was conducted using two-way ANOVA with a Tukey/Bonferroni post-hoc test. Significant differences are indicated by *P<0.05.

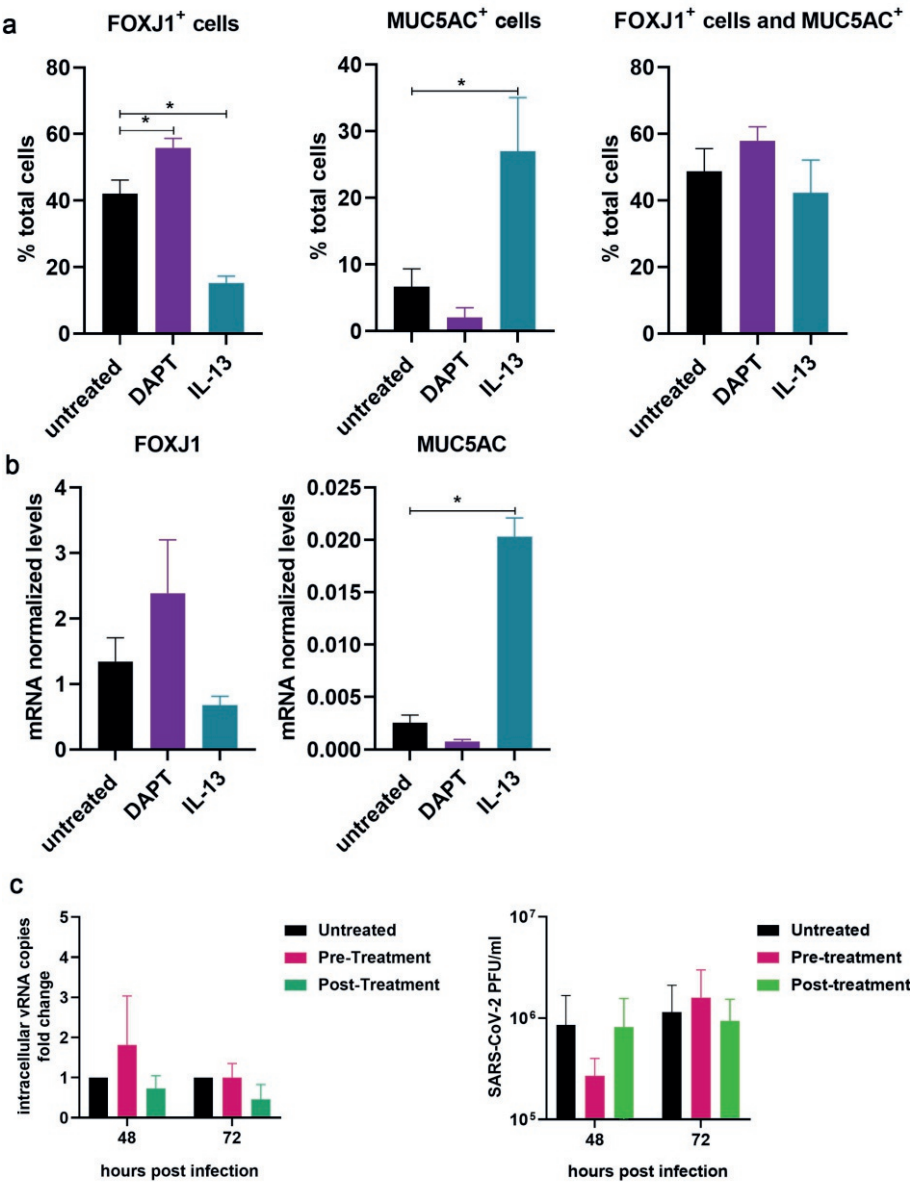

Figure S2: Effect of long-term DAPT/IL-13 exposure on epithelial cell composition and effect of acute DAPT/IL-13 exposure on susceptibility to SARS-CoV-2 infection. ALI-PBEC (mix of 4-5 donors) were differentiated for 3 weeks, before addition of DAPT (5 µM) or IL-13 (1 ng/ml), followed by differentiation for an additional 2 weeks. (a) After 5 weeks of differentiation, ALI-PBEC were fixed, stained and analyzed by immunofluorescence using primary antibodies against MUC5AC and FOXJ1 (goblet cell marker, ciliated cell marker) in combination with DAPI for nuclear staining. The quantification of FOXJ1-positive cells and MUC5AC-positive cells was done by ImageJ software. Data are mean ± SEM. (b) mRNA levels of *FOXJ1* and *MUC5AC* were measured by RT-qPCR. Data are mean ± SEM. Analysis of differences was conducted using paired t test. (c) Short-term treatment with DAPT was

performed in cells after 5 weeks of differentiation. Cells were either pre-treated with DAPT for 24 h (pre-treatment) or post-treated directly after infection (post-treatment). Intracellular SARS-CoV-2 RNA copies were measured by RT-qPCR and plaque assay was performed with apical washes to quantify infectious virus titers. n=3 independent experiments. Data are mean ± SEM. Fold change in intracellular RNA copies was compared to untreated controls. Statistical analysis was performed using a paired t test. Significant differences are indicated by *P<0.05.

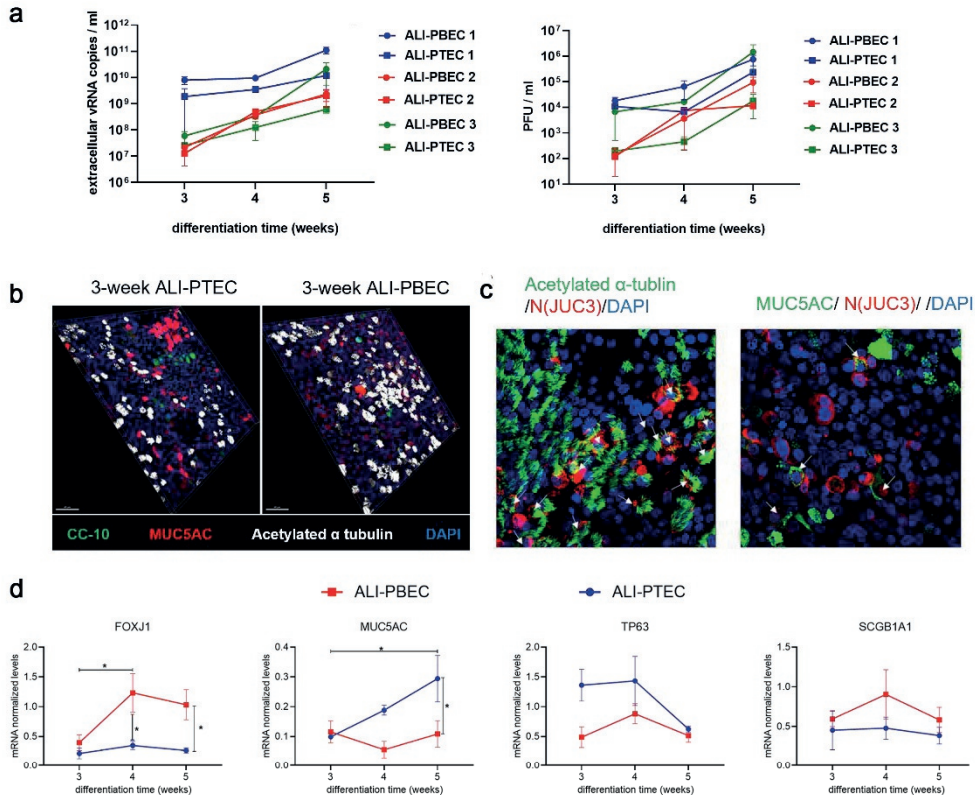

Figure S3: Effect of culture duration on infection and epithelial cell-specific genes in PTEC and PBEC. (a) Extracellular viral RNA copies in the apical wash were measured by RT-qPCR and viral infectious progeny was determined by plaque assay in Vero E6 cells. Mean values ± SEM is presented from 3 independent experiments using 3 different donor mixes. (b) Immunofluorescence staining of PTEC and PBEC with antibodies against CC-10 (Club cell marker), MUC5AC (goblet cell marker), acetylated α-tubulin (ciliated cell marker) in combination with DAPI for nuclear staining. (c) Immunofluorescence staining of PTEC with antibodies against acetylated α-tubulin and SARS-CoV-2 N protein in combination with DAPI. Immunofluorescence images shown are representative merged z-stack images for results of 3 independent experiments with 630 x original magnification. (d) ALI-PTEC/PBEC (mix of 5 donors) were differentiated at ALI for 3, 4 or 5 weeks, and analyzed by RT-qPCR to measure gene expression of FOXJ1 (ciliated cell marker), MUC5AC (goblet cell marker), SCGB1A1 (club cell marker) and TP63 (basal cell marker). n=3 independent experiments at 3-5 weeks derived from three donor mixes the same as used in Fig.3. Data are mean ± SEM. Analysis of differences was conducted using two-way ANOVA with a Tukey/Bonferroni post-hoc test. Significant differences are indicated by *P<0.05.

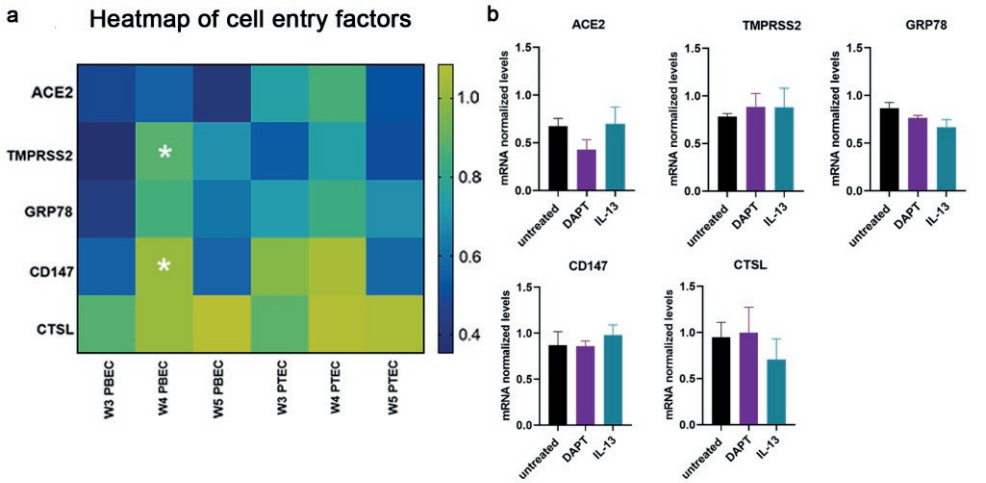

Figure S4: Effect of culture duration and DAPT/IL13 treatment on expression of SARS-CoV-2 cell-entry factors. (a) Analysis of gene expression of viral cell-entry factors by RT-qPCR in 3, 4 and 5 week uninfected cultures of PTEC and PBEC and (b) in DAPT or IL-13 treated 5 week-differentiated cultures. Data are mean values ± SEM. n=3 independent experiments derived from three donor mixes. Statistical analysis was conducted using two-way ANOVA with a Tukey post-hoc test or one-way ANOVA with Dunnett test. Significant differences are indicated by $P<0.05$. *= 5-week ALI-PBEC vs 3-week ALI-PBEC.

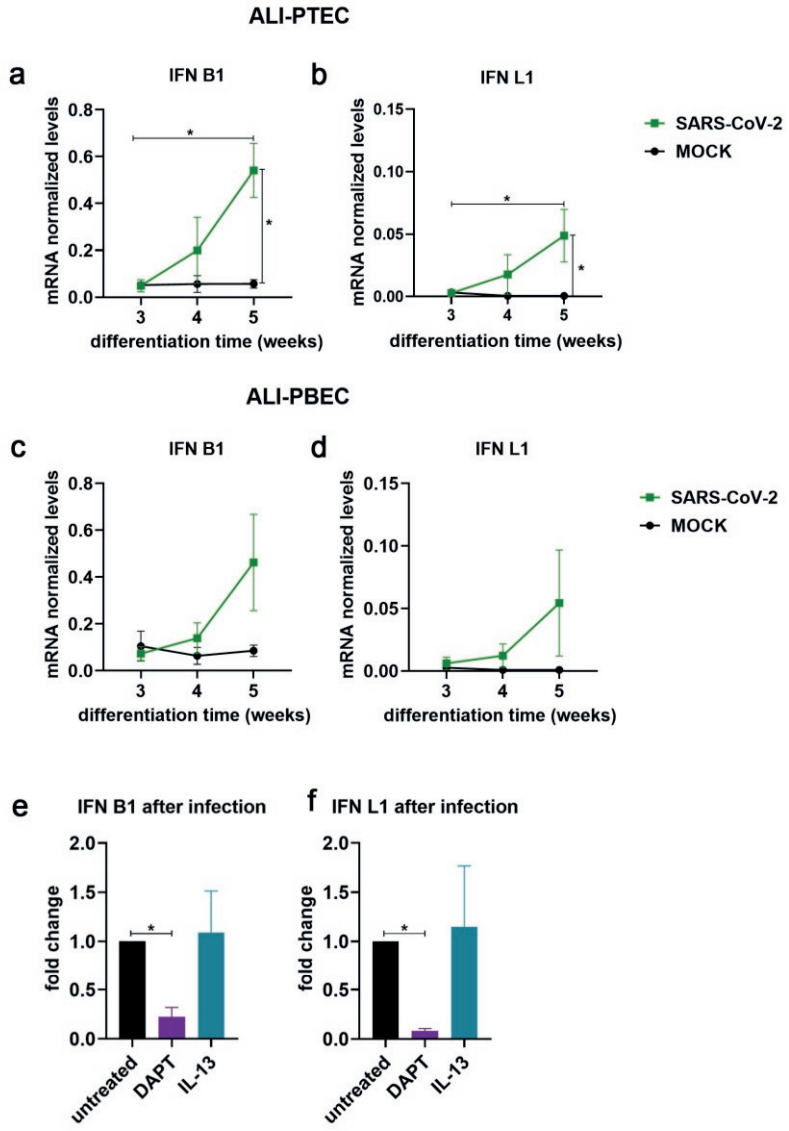

Figure S5: Antiviral responses after SARS-CoV-2 infection. ALI-PTEC and PBEC cultured for 3-5 weeks (A-D), and 5-week ALI-PBEC (E, F) cultured at ALI in presence or absence of DAPT or IL-13 (during the last 2 weeks), were infected by SARS-CoV-2 (30,000 PFU per insert). Cells were lysed at 72 hpi to quantify mRNA levels of *IFNB1* (a/c/e) and *IFNL1* (b/d/f) by RT-qPCR. n=3 independent experiments using 3 different donor mixes. Data are mean ± SEM. Fold change in E and F was compared to untreated controls. Analysis of differences was conducted using two-way ANOVA with a Tukey/Bonferroni post-hoc test. Significant differences are indicated by *P<0.05.

Table S1: The differentially expressed genes in ALI-PBEC and ALI-PTEC between 3-week and 5-week cultures

Gene symbol	logFC	logCPM	F	P value	FDR
ALI-PBEC					
GBP1	1,002649	5,59286	28,42654	0,000205	0,011999
C6	1,008593	4,598683	34,17632	9,24E-05	0,011252
FAM13C	1,01462	1,686769	15,42701	0,002161	0,028787
NMNAT2	1,040247	2,463503	27,22633	0,000245	0,012624
VEPH1	1,040893	1,215865	12,34508	0,004528	0,04146
KIF26B	1,047462	2,465433	23,28812	0,000464	0,01499
SUSD5	1,048884	0,593884	13,23716	0,003618	0,037666
ALS2CR12	1,052709	3,056197	27,67302	0,000229	0,012344
TEKT3	1,073256	0,717851	21,28602	0,000662	0,017229
ADH7	1,076298	6,748417	33,31955	0,000103	0,011252
SLC1A1	1,077068	5,080468	21,27037	0,000663	0,017229
GCNT4	1,079011	1,61263	23,97091	0,000414	0,014456
GNA14	1,082498	2,955824	12,76014	0,004075	0,039248
SERPING1	1,083826	3,388572	23,87261	0,000421	0,014456
CXCL3	1,087681	3,835865	9,254044	0,010664	0,06513
LINC00689	1,101837	1,213377	7,917803	0,016176	0,081168
RP11-356I2.4	1,122523	0,167388	18,21206	0,001194	0,022104
CCL20	1,124136	4,278383	10,84357	0,006751	0,051083
CCDC173	1,129108	4,661543	32,15727	0,000121	0,011477
SFRP2	1,130373	1,308617	10,19488	0,008098	0,056111
ARG2	1,131078	2,939088	13,98017	0,003021	0,034592
GLYATL2	1,139479	0,778915	13,64786	0,003273	0,036107
ZNF853	1,145346	0,872255	7,059498	0,021529	0,095652
ACTBL2	1,146252	1,202529	14,67346	0,002567	0,031485
OXGR1	1,154019	0,362324	8,221797	0,01467	0,077218
TM6SF1	1,157709	0,157218	15,9499	0,001924	0,026801
ZSCAN12P1	1,177114	0,305378	10,76975	0,00689	0,051681
AFAP1L2	1,184962	2,2387	12,23583	0,004657	0,042023
UCHL1	1,187467	1,02622	11,45645	0,005715	0,046538
UCA1	1,203382	2,242207	8,053701	0,015481	0,079529
DMBT1	1,214279	5,708363	29,85375	0,000166	0,011477

CES1	1,220755	5,121919	37,27795	6,28E-05	0,010533
SLC5A1	1,231942	3,193087	47,33052	2,09E-05	0,007842
RP11-642P15.1	1,25914	0,94976	23,23305	0,000469	0,015018
EEF1A2	1,292066	1,559594	6,937111	0,022454	0,098292
RP1-27K12.2	1,303139	2,755264	16,99273	0,001536	0,024375
IL22RA1	1,313443	0,205781	11,12312	0,006253	0,048826
HLA-DQA1	1,318172	3,113733	9,05018	0,01134	0,067178
CYP24A1	1,330907	3,752493	8,916734	0,011811	0,068671
RGS22	1,388349	3,30457	31,34144	0,000135	0,011477
SLC6A20	1,427783	2,039617	23,02251	0,000486	0,015242
MAP1B	1,430696	3,968576	17,9179	0,001267	0,022561
CTSV	1,492403	3,621686	16,42133	0,001736	0,025711
NCR3LG1	1,550185	1,734731	35,59817	7,72E-05	0,011007
CXCL5	1,557573	3,176724	9,935025	0,008726	0,058225
CHI3L1	1,576727	1,837262	20,73273	0,000732	0,017984
GPNMB	1,699773	6,046425	14,86666	0,002455	0,030665
AL121901.1	1,810156	1,657353	10,00457	0,008553	0,05784
SLC5A8	1,836587	1,7187	17,35876	0,001422	0,023594
SPTBN4	-2,09053	2,377134	25,71497	0,000311	0,013732
AC022596.6	-2,0531	2,060019	15,32716	0,00221	0,029127
EXOC3L1	-1,82355	1,023619	14,22714	0,002849	0,033538
PLCD4	-1,76792	1,754185	22,92399	0,000494	0,015302
IQGAP3	-1,7452	0,909495	11,2558	0,006032	0,047916
LGALS7	-1,70892	4,387691	19,0473	0,00101	0,020535
LGALS7B	-1,69201	3,76449	26,46105	0,000276	0,013273
CYP26C1	-1,64831	1,05923	15,95419	0,001922	0,026801
CYP4F23P	-1,6461	2,028523	12,52156	0,004328	0,040383
ASPM	-1,63808	1,457722	11,77712	0,005249	0,044623
PLA2G4F	-1,63644	2,389311	11,3363	0,005903	0,047229
PDE11A	-1,60907	3,468886	10,12901	0,008252	0,056692
MAOB	-1,57209	1,719884	19,53167	0,000919	0,020088
KRT13	-1,5713	8,159369	17,33201	0,00143	0,023671
WNT10A	-1,55668	5,014215	88,11726	9,64E-07	0,00322
KLK7	-1,52867	4,871598	17,55299	0,001366	0,023371
MYOT	-1,49218	1,383578	12,49269	0,00436	0,040602

ALOX15B	-1,42438	4,068088	30,08054	0,000161	0,011477
CKAP2L	-1,42374	0,387569	7,749934	0,017085	0,083565
KCNE4	-1,40436	1,775868	12,70016	0,004137	0,039553
KLK8	-1,38961	1,394874	27,35364	0,000241	0,012533
EFS	-1,32513	1,430937	16,95673	0,001548	0,024423
COL7A1	-1,29595	7,750315	40,8237	4,15E-05	0,009439
MEGF6	-1,28014	4,888583	28,19833	0,000212	0,012091
CYP26B1	-1,27924	7,61654	9,465685	0,010011	0,063124
PLCH2	-1,27526	6,836023	48,42031	1,87E-05	0,007842
RP5-1085F17.3	-1,26647	0,327113	18,20274	0,001196	0,022104
TNNI2	-1,26069	4,253661	11,14312	0,006219	0,048644
RP11-235E17.6	-1,26026	2,578247	19,50609	0,000924	0,020119
FGFR3	-1,25858	7,297273	110,6972	2,94E-07	0,001553
EGFL6	-1,24513	3,665653	12,44813	0,00441	0,040906
HMHA1	-1,24382	3,55872	7,978989	0,015858	0,080375
MMP28	-1,24275	5,290207	45,78856	2,44E-05	0,008486
GPT	-1,23928	0,373352	12,28928	0,004593	0,041765
CLEC2D	-1,23812	1,918601	19,119	0,000996	0,020423
RHBDL1	-1,23676	2,113606	19,16153	0,000988	0,020339
ECM1	-1,22886	4,151404	12,24362	0,004648	0,042017
MEX3B	-1,22089	1,358241	8,708329	0,012593	0,071092
RP11-268J15.5	-1,20935	2,56421	22,61057	0,000522	0,01548
CYP2T2P	-1,20801	6,446988	21,97836	0,000584	0,016352
FAM229A	-1,20618	2,868697	20,50802	0,000764	0,018271
CSRNP3	-1,20084	1,439979	11,40015	0,005802	0,046872
PCP2	-1,20062	0,595494	7,173733	0,020707	0,093452
PLK1	-1,19771	1,865708	17,22768	0,001462	0,023788
CAPNS2	-1,19411	1,982033	11,36996	0,00585	0,046994
ADIRF	-1,19009	3,253925	34,07615	9,36E-05	0,011252
PTTG1	-1,18856	3,121655	32,07054	0,000122	0,011477
BDKRB1	-1,17456	0,394196	17,47789	0,001387	0,023391
GHR	-1,17168	0,534359	9,381281	0,010266	0,063814
ANKRD9	-1,16422	4,305996	25,46552	0,000324	0,01378
FOXN4	-1,16263	3,312565	11,79335	0,005226	0,044623
HSD11B2	-1,15791	4,53207	14,92014	0,002425	0,030371

IGFBP6	-1,15351	7,240489	108,5039	3,27E-07	0,001553
KRT14	-1,14903	4,978784	10,55921	0,007306	0,05301
RP11-44N21.1	-1,14886	0,745321	11,82374	0,005185	0,044414
VMO1	-1,14822	7,730684	34,33033	9,06E-05	0,011252
NAPSA	-1,14532	0,73691	9,183362	0,010893	0,065801
KCP	-1,14261	2,294007	29,44502	0,000176	0,011598
WFDC3	-1,14259	2,556692	10,05651	0,008426	0,057345
CENPE	-1,14219	1,280905	7,721378	0,017246	0,084056
CFD	-1,13951	3,218426	14,73457	0,002531	0,031258
TMEM160	-1,13884	3,549933	30,43181	0,000153	0,011477
SNCG	-1,13843	2,811491	21,10013	0,000684	0,017421
AIFM3	-1,13564	2,050572	11,13285	0,006237	0,048753
RBBP8NL	-1,1341	3,470603	18,30167	0,001172	0,021877
CTU1	-1,12955	2,727798	17,31734	0,001435	0,023671
ABCC9	-1,12894	4,376523	24,04358	0,000409	0,014456
KLK6	-1,12721	3,030986	9,409648	0,01018	0,063582
RP11-108K14.4	-1,12421	3,403741	47,91893	1,97E-05	0,007842
FES	-1,12125	2,078394	17,20445	0,001469	0,023788
HSPB1	-1,11756	8,551601	77,27061	1,89E-06	0,004484
PRSS3	-1,11568	1,316268	9,743191	0,009226	0,060129
CHRM3	-1,11185	2,125622	11,38383	0,005828	0,046894
POU5F1	-1,11076	3,685524	8,312625	0,014253	0,076077
CDCA3	-1,10493	0,745953	9,322954	0,010446	0,064373
LIME1	-1,10456	2,077558	16,8718	0,001576	0,024625
UNC5CL	-1,10099	1,164797	9,878959	0,008869	0,058684
RP11-538D16.2	-1,10034	1,293376	10,81006	0,006814	0,051351
AC009061.1	-1,0961	2,198033	15,63168	0,002064	0,027967
NDUFA13	-1,08936	1,374798	11,11447	0,006268	0,048826
UCN2	-1,08535	1,380242	17,16759	0,00148	0,023892
GPS2	-1,08416	1,109488	8,343	0,014117	0,075712
ANKRD2	-1,08102	0,646797	7,804956	0,016781	0,082601
CYP2E1	-1,07754	2,401679	19,55921	0,000915	0,020032
HES6	-1,07393	4,396359	24,81671	0,00036	0,014136
RP5-1074L1.4	-1,07384	1,133285	8,676116	0,012719	0,071522
HCN3	-1,07207	2,945652	33,76532	9,75E-05	0,011252

NYAP1	-1,06774	-0,30713	8,367067	0,01401	0,075365
ADAMTSL4	-1,06769	4,669001	8,592351	0,013055	0,072607
C19orf40	-1,06529	0,537614	9,758387	0,009185	0,059996
LTBP4	-1,06463	6,480215	36,66196	6,76E-05	0,010608
KIFC1	-1,06155	0,992713	7,844801	0,016564	0,082067
ADAMTSL5	-1,05223	3,977505	18,22178	0,001191	0,022104
FAM173A	-1,04914	3,761411	38,47602	5,44E-05	0,01008
C12orf54	-1,0457	0,473343	8,517447	0,013363	0,07355
AP001053.11	-1,045	1,784287	18,49842	0,001127	0,021576
WNT2B	-1,04208	1,98975	16,13253	0,001848	0,02628
KDR	-1,03952	3,400876	12,14524	0,004767	0,042533
IQCJ-SCHIP1	-1,03685	0,963322	14,41452	0,002726	0,03274
NFATC4	-1,03594	5,418897	22,16864	0,000564	0,016106
PRKCDBP	-1,03538	4,92231	34,12324	9,31E-05	0,011252
PRICKLE4	-1,03464	6,185696	30,46854	0,000152	0,011477
SPINK5	-1,0342	4,561195	11,50763	0,005638	0,046276
DLK2	-1,03399	3,666093	33,64215	9,91E-05	0,011252
PLEKHH3	-1,03309	6,09077	109,4289	3,12E-07	0,001553
PPP1R35	-1,03304	3,717862	16,69999	0,001635	0,024991
FLG-AS1	-1,02837	3,84126	15,16394	0,002294	0,029745
BRICD5	-1,02297	2,700028	13,73493	0,003204	0,035576
TNFRSF25	-1,02002	4,588371	44,42559	2,81E-05	0,008905
TRIM7	-1,01838	3,731958	39,00875	5,11E-05	0,009989
PTMS	-1,01763	6,404615	33,33356	0,000103	0,011252
RP11-783K16.13	-1,01354	1,096157	13,9964	0,00301	0,034487
CTD-3214H19.6	-1,01297	0,204872	7,51536	0,018461	0,087378
PCDHB15	-1,01281	1,23667	16,91976	0,00156	0,024465
RP11-258C19.7	-1,01247	1,280704	11,74446	0,005294	0,044769
PHYHIP	-1,01103	4,106824	36,22729	7,14E-05	0,010778
AC005262.2	-1,00651	1,244988	8,153251	0,014995	0,078099
ZNF648	-1,00603	3,002909	13,40844	0,003469	0,036849
DBP	-1,00518	4,433981	24,40215	0,000385	0,014257
GDPD3	-1,00033	2,191338	19,86287	0,000863	0,019631

Gene symbol	logFC	logCPM	F	P value	FDR
ALI-PTEC					
DMBT1	1,003702	5,708363	20,07165	0,000829	0,076555
ANKFN1	1,03626	3,177326	26,0421	0,000295	0,067598
RP11-247L20.4	1,03854	0,903807	17,57343	0,00136	0,084818
CCDC173	1,040203	4,661543	24,83022	0,000359	0,067598
NCR3LG1	1,075958	1,734731	14,66594	0,002571	0,091098
VNN3	1,102569	2,739779	20,95719	0,000703	0,075288
PTPRT	1,121797	3,408321	44,66975	2,74E-05	0,0534
AC005281.1	1,152108	1,904765	15,93077	0,001932	0,089116
FAM167A	1,160504	1,696483	18,33648	0,001164	0,081002
DSCAML1	1,161098	1,538778	18,19868	0,001197	0,082086
PLA1A	1,165826	1,232803	17,35953	0,001422	0,085482
RND2	1,188845	2,016029	16,12771	0,00185	0,088906
SUSD5	1,195827	0,593884	16,28759	0,001787	0,088694
DAAM2	1,200075	1,531415	15,37768	0,002185	0,090206
COL28A1	1,231637	3,080218	27,89596	0,000222	0,062312
USH1C	1,28638	1,140772	19,77719	0,000877	0,076555
TMEM176B	1,310352	2,70275	25,33272	0,000331	0,067598
CES1	1,319449	5,121919	39,111	5,05E-05	0,0534
VEPH1	1,330778	1,215865	14,55405	0,002639	0,091701
RGS22	1,340184	3,30457	26,62032	0,00027	0,06463
CXCL6	1,348396	4,33736	29,33268	0,000179	0,062312
CCL20	1,381199	4,278383	16,82882	0,00159	0,087603
RP11-642P15.1	1,387534	0,94976	18,68823	0,001085	0,080108
TMEM176A	1,425233	2,424882	39,54631	4,80E-05	0,0534
TCHH	1,429566	2,34236	21,01183	0,000696	0,075219
MACROD2	1,458391	1,356867	23,45164	0,000452	0,067598
BDNF	1,499378	0,727706	14,38546	0,002745	0,092443
GRM7	1,534808	2,010926	35,11407	8,20E-05	0,0534
CYP2A13	1,6437	4,77677	14,5103	0,002666	0,092091
CHI3L1	1,645907	1,837262	24,19878	0,000398	0,067598
CXCL5	2,16049	3,176724	19,96095	0,000847	0,076555
SLC5A8	2,198774	1,7187	23,7566	0,000429	0,067598
IQGAP3	-2,59342	0,909495	22,71009	0,000513	0,068158

ASPM	-1,89113	1,457722	15,38539	0,002181	0,090206
KLK7	-1,83656	4,871598	25,61704	0,000316	0,067598
CENPE	-1,78737	1,280905	17,97174	0,001253	0,082286
FBXO24	-1,41878	0,139514	16,18092	0,001829	0,088694
ARHGAP11B	-1,39201	1,100907	25,09047	0,000344	0,067598
PLCD4	-1,36981	1,754185	14,04437	0,002975	0,096749
MAOB	-1,32147	1,719884	16,32054	0,001774	0,088694
ECM1	-1,31965	4,151404	15,93715	0,001929	0,089116
LGALS7B	-1,2755	3,76449	16,05833	0,001878	0,089116
UCN2	-1,26972	1,380242	24,58247	0,000374	0,067598
LMNB1	-1,23352	2,202663	15,1922	0,002279	0,090908
KRT14	-1,23213	4,978784	15,69549	0,002035	0,090206
GPR37L1	-1,19404	2,34757	29,30917	0,00018	0,062312
MAP2	-1,18982	2,346671	23,38027	0,000457	0,067598
TENM2	-1,1629	2,100679	21,7164	0,000612	0,070391
RP4-758J18.10	-1,14543	0,954296	14,1606	0,002894	0,094976
NXPH4	-1,12633	2,059991	20,22591	0,000805	0,076555
RHBDL1	-1,11214	2,113606	15,52982	0,002112	0,090206
SEMA6A	-1,1117	2,970364	21,65018	0,000619	0,070391
ALDOC	-1,10159	4,805836	15,56031	0,002097	0,090206
ALOX15B	-1,09932	4,068088	20,08179	0,000828	0,076555
CA9	-1,04728	3,850175	37,16396	6,36E-05	0,0534
FIBIN	-1,03703	1,317875	15,218	0,002266	0,090908
CLDN8	-1,01129	4,270443	18,61824	0,0011	0,080108
WNT10A	-1,01129	5,014215	39,60865	4,77E-05	0,0534

References

1. Chakraborty I, Maity P. COVID-19 outbreak: Migration, effects on society, global environment and prevention. Sci Total Environ. 2020 Aug 1;728:138882.
2. Toyoshima Y, Nemoto K, Matsumoto S, Nakamura Y, Kiyotani K. SARS-CoV-2 genomic variations associated with mortality rate of COVID-19. J Hum Genet. 2020 Dec;65(12):1075-82.
3. Yurkovetskiy L, Wang X, Pascal KE, Tomkins-Tinch C, Nyalile TP, Wang Y, et al. Structural and Functional Analysis of the D614G SARS-CoV-2 Spike Protein Variant. Cell. 2020 Oct 29;183(3):739-51.e8.
4. Trevisan C, Noale M, Prinelli F, Maggi S, Sojic A, Di Bari M, et al. Age-Related Changes in Clinical Presentation of Covid-19: the EPICOVID19 Web-Based Survey. Eur J Intern Med. 2021;86:41-47.
5. Alwani M, Yassin A, Al-Zoubi RM, Aboumarzouk OM, Nettleship J, Kelly D, et al. Sex-based differences in severity and mortality in COVID-19. Rev Med Virol. 2021 Nov;31(6):e2223.
6. Yu W, Rohli KE, Yang S, Jia P. Impact of obesity on COVID-19 patients. J Diabetes Complications. 2021 Mar;35(3):107817.
7. Carraturo F, Del Giudice C, Morelli M, Cerullo V, Libralato G, Galdiero E, et al. Persistence of SARS-CoV-2 in the environment and COVID-19 transmission risk from environmental matrices and surfaces. Environ Pollut. 2020 Oct;265(Pt B):115010.
8. Bansal M. Cardiovascular disease and COVID-19. Diabetes Metab Syndr. 2020 May-Jun;14(3):247-50.
9. Ovsyannikova IG, Haralambieva IH, Crooke SN, Poland GA, Kennedy RB. The role of host genetics in the immune response to SARS-CoV-2 and COVID-19 susceptibility and severity. Immunol Rev. 2020;296(1):205-19.
10. Park SE. Epidemiology, virology, and clinical features of severe acute respiratory syndrome -coronavirus-2 (SARS-CoV-2; Coronavirus Disease-19). Clin Exp Pediatr. 2020 4;63(4):119-24.
11. Zhou P, Yang X-L, Wang X-G, Hu B, Zhang L, Zhang W, et al. A pneumonia outbreak associated with a new coronavirus of probable bat origin. Nature. 2020 2020/03/01;579(7798):270-73.
12. Hiemstra PS, McCray PB, Jr., Bals R. The innate immune function of airway epithelial cells in inflammatory lung disease. Eur Respir J. 2015 Apr;45(4):1150-62.
13. Iwasaki A, Foxman EF, Molony RD. Early local immune defences in the respiratory tract. Nat Rev Immunol. 2017 Jan;17(1):7-20.
14. Iwasaki A, Foxman EF, Molony RD. Early local immune defences in the respiratory tract. Nature Reviews Immunology. 2017 2017/01/01;17(1):7-20.
15. Bovard D, Giralt A, Trivedi K, Neau L, Kanellos P, Iskandar A, et al. Comparison of the basic morphology and function of 3D lung epithelial cultures derived from several donors. Curr Res Toxicol. 2020 Jun 10;1:56-69.
16. Belgacemi R, Luczka E, Ancel J, Diabasana Z, Perotin JM, Germain A, et al. Airway epithelial cell differentiation relies on deficient Hedgehog signalling in COPD. EBioMedicine. 2020 Jan;51:102572.
17. Leung C, Wadsworth SJ, Yang SJ, Dorscheid DR. Structural and functional variations in human bronchial epithelial cells cultured in air-liquid interface using different growth media. American journal of physiology Lung cellular and molecular physiology. 2020 May 1;318(5):L1063-l73.
18. Hou YJ, Okuda K, Edwards CE, Martinez DR, Asakura T, Dinnon KH, 3rd, et al. SARS-CoV-2 Reverse Genetics Reveals a Variable Infection Gradient in the Respiratory Tract. Cell. 2020 Jul 23;182(2):429-46.e14.
19. Hao S, Ning K, Kuz CA, Vorhies K, Yan Z, Qiu J. Long-Term Modeling of SARS-CoV-2 Infection of In Vitro Cultured Polarized Human Airway Epithelium. mBio. 2020 Nov 6;11(6).

20. Zhu N, Wang W, Liu Z, Liang C, Wang W, Ye F, et al. Morphogenesis and cytopathic effect of SARS-CoV-2 infection in human airway epithelial cells. Nat Commun. 2020 Aug 6;11(1):3910.
21. Ehre C. SARS-CoV-2 Infection of Airway Cells. N Engl J Med. 2020 Sep 3;383(10):969.
22. Aguiar JA, Tremblay BJ, Mansfield MJ, Woody O, Lobb B, Banerjee A, et al. Gene expression and in situ protein profiling of candidate SARS-CoV-2 receptors in human airway epithelial cells and lung tissue. Eur Respir J. 2020 Sep;56(3).
23. Hoffmann M, Kleine-Weber H, Schroeder S, Krüger N, Herrler T, Erichsen S, et al. SARS-CoV-2 Cell Entry Depends on ACE2 and TMPRSS2 and Is Blocked by a Clinically Proven Protease Inhibitor. Cell. 2020 Apr 16;181(2):271-80.e8.
24. Sungnak W, Huang N, Bécavin C, Berg M, Queen R, Litvinukova M, et al. SARS-CoV-2 entry factors are highly expressed in nasal epithelial cells together with innate immune genes. Nat Med. 2020 May;26(5):681-87.
25. Wang S, Qiu Z, Hou Y, Deng X, Xu W, Zheng T, et al. AXL is a candidate receptor for SARS-CoV-2 that promotes infection of pulmonary and bronchial epithelial cells. Cell Research. 2021 2021/01/08.
26. Lukassen S, Chua RL, Trefzer T, Kahn NC, Schneider MA, Muley T, et al. SARS-CoV-2 receptor ACE2 and TMPRSS2 are primarily expressed in bronchial transient secretory cells. Embo j. 2020 May 18;39(10):e105114.
27. Bridges JP, Vladar EK, Huang H, Mason RJ. Respiratory epithelial cell responses to SARS-CoV-2 in COVID-19. 2022;Thorax 77(2):203-09.
28. Mulay A, Konda B, Garcia G, Jr., Yao C, Beil S, Villalba JM, et al. SARS-CoV-2 infection of primary human lung epithelium for COVID-19 modeling and drug discovery. Cell reports. 2021;35(5):109055-55.
29. Salgado-Benvindo C, Thaler M, Tas A, Ogando NS, Bredenbeek PJ, Ninaber DK, et al. Suramin Inhibits SARS-CoV-2 Infection in Cell Culture by Interfering with Early Steps of the Replication Cycle. Antimicrob Agents Chemother. 2020 Jul 22;64(8).
30. Huang J, Hume AJ, Abo KM, Werder RB, Villacorta-Martin C, Alysandratos KD, et al. SARS-CoV-2 Infection of Pluripotent Stem Cell-Derived Human Lung Alveolar Type 2 Cells Elicits a Rapid Epithelial-Intrinsic Inflammatory Response. Cell Stem Cell. 2020 Dec 3;27(6):962-73.e7.
31. Katsura H, Sontake V, Tata A, Kobayashi Y, Edwards CE, Heaton BE, et al. Human Lung Stem Cell-Based Alveolospheres Provide Insights into SARS-CoV-2-Mediated Interferon Responses and Pneumocyte Dysfunction. Cell Stem Cell. 2020 Dec 3;27(6):890-904.e8.
32. Lukassen S, Chua RL, Trefzer T, Kahn NC, Schneider MA, Muley T, et al. SARS-CoV-2 receptor ACE2 and TMPRSS2 are primarily expressed in bronchial transient secretory cells. EMBO J. 2020;39(10):e105114-e14.
33. Mertens TCJ, van der Does AM, Kistemaker LE, Ninaber DK, Taube C, Hiemstra PS. Cigarette smoke differentially affects IL-13-induced gene expression in human airway epithelial cells. Physiological reports. 2017 Jul;5(13).
34. Amatngalim GD, Schrumpf JA, Dishchekenian F, Mertens TCJ, Ninaber DK, van der Linden AC, et al. Aberrant epithelial differentiation by cigarette smoke dysregulates respiratory host defence. Eur Respir J. 2018 Apr;51(4).
35. Wang Y, Ninaber DK, van Schadewijk A, Hiemstra PS. Tiotropium and Fluticasone Inhibit Rhinovirus-Induced Mucin Production via Multiple Mechanisms in Differentiated Airway Epithelial Cells. Front Cell Infect Microbiol. 2020;10:278.
36. Zhang H, Rostami MR, Leopold PL, Mezey JG, O'Beirne SL, Strulovici-Barel Y, et al. Expression of the SARS-CoV-2 ACE2 Receptor in the Human Airway Epithelium. American journal of respiratory and critical care medicine. 2020 Jul 15;202(2):219-29.

37. Lieberman NAP, Peddu V, Xie H, Shrestha L, Huang M-L, Mears MC, et al. In vivo antiviral host transcriptional response to SARS-CoV-2 by viral load, sex, and age. PLOS Biology. 2020;18(9):e3000849.
38. Vanderheiden A, Ralfs P, Chirkova T, Upadhyay AA, Zimmerman MG, Bedoya S, et al. Type I and Type III Interferons Restrict SARS-CoV-2 Infection of Human Airway Epithelial Cultures. 2020;94(19):e00985-20.
39. Liao Y, Li X, Mou T, Zhou X, Li D, Wang L, et al. Distinct infection process of SARS-CoV-2 in human bronchial epithelial cell lines. J Med Virol. 2020 Nov;92(11):2830-38.
40. Bost P, Giladi A, Liu Y, Bendjelal Y, Xu G, David E, et al. Host-Viral Infection Maps Reveal Signatures of Severe COVID-19 Patients. Cell. 2020 2020/06/25/;181(7):1475-88.e12.
41. Ziegler CGK, Allon SJ, Nyquist SK, Mbano IM, Miao VN, Tzouanas CN, et al. SARS-CoV-2 Receptor ACE2 Is an Interferon-Stimulated Gene in Human Airway Epithelial Cells and Is Detected in Specific Cell Subsets across Tissues. Cell. 2020;181(5):1016-35.e19.
42. Ruiz García S, Deprez M, Lebrigand K, Cavard A, Paquet A, Arguel MJ, et al. Novel dynamics of human mucociliary differentiation revealed by single-cell RNA sequencing of nasal epithelial cultures. Development. 2019 Oct 23;146(20).
43. Vieira Braga FA, Kar G, Berg M, Carpaij OA, Polanski K, Simon LM, et al. A cellular census of human lungs identifies novel cell states in health and in asthma. Nature Medicine. 2019 2019/07/01;25(7):1153-63.
44. Kimura H, Francisco D, Conway M, Martinez FD, Vercelli D, Polverino F, et al. Type 2 inflammation modulates ACE2 and TMPRSS2 in airway epithelial cells. J Allergy Clin Immunol. 2020 Jul;146(1):80-88.e8.
45. Eger K, Bel EH. Asthma and COVID-19: do we finally have answers? Eur Respir J. 2021 Mar;57(3).
46. Bonser LR, Eckalbar WL, Rodriguez L, Shen J, Koh KD, Ghias K, et al. The Type 2 Asthma Mediator IL-13 Inhibits Severe Acute Respiratory Syndrome Coronavirus 2 Infection of Bronchial Epithelium. 2022; AM J Respir Cell Mol Biol. 66(4):391-401.
47. Morrison CB, Edwards CE, Shaffer KM, Araba KC, Wykoff JA, Williams DR, et al. SARS-CoV-2 infection of airway cells causes intense viral and cell shedding, two spreading mechanisms affected by IL-13. Proceedings of the National Academy of Sciences of the United States of America. 2022 Apr 19;119(16):e2119680119.
48. Liu Y, Lv J, Liu J, Li M, Xie J, Lv Q, et al. Mucus production stimulated by IFN-AhR signaling triggers hypoxia of COVID-19. Cell Res. 2020 Dec;30(12):1078-87.
49. Ravindra NG, Alfajaro MM, Gasque V, Huston NC, Wan H, Szigeti-Buck K, et al. Single-cell longitudinal analysis of SARS-CoV-2 infection in human airway epithelium identifies target cells, alterations in gene expression, and cell state changes. PLoS Biol. 2021 Mar;19(3):e3001143.
50. Zhao M-M, Yang W-L, Yang F-Y, Zhang L, Huang W-J, Hou W, et al. Cathepsin L plays a key role in SARS-CoV-2 infection in humans and humanized mice and is a promising target for new drug development. Signal Transduction and Targeted Therapy. 2021 2021/03/27;6(1):134.
51. Hui KPY, Ho JCW, Cheung MC, Ng KC, Ching RHH, Lai KL, et al. SARS-CoV-2 Omicron variant replication in human bronchus and lung ex vivo. Nature. 2022 Mar;603(7902):715-20.
52. Liu Y, Liu J, Johnson BA, Xia H, Ku Z, Schindewolf C, et al. Delta spike P681R mutation enhances SARS-CoV-2 fitness over Alpha variant. Cell Reports. 2022 2022/05/17/;39(7):110829.
53. Mache C, Schulze J, Holland G, Bourquain D, Gensch J-M, Oh D-Y, et al. SARS-CoV-2 Omicron variant is attenuated for replication in a polarized human lung epithelial cell model. Communications Biology. 2022 2022/10/27;5(1):1138.

54. Schrumpf JA, Ninaber DK, van der Does AM, Hiemstra PS. TGF-β1 Impairs Vitamin D-Induced and Constitutive Airway Epithelial Host Defense Mechanisms. Journal of innate immunity. 2020;12(1):74-89.
55. Kovacikova K, Morren BM, Tas A, Albulescu IC, van Rijswijk R, Jarhad DB, et al. 6'-β-Fluoro-Homoaristeromycin and 6'-Fluoro-Homoneplanocin A Are Potent Inhibitors of Chikungunya Virus Replication through Their Direct Effect on Viral Nonstructural Protein 1. Antimicrob Agents Chemother. 2020 Mar 24;64(4).
56. Corman VM, Landt O, Kaiser M, Molenkamp R, Meijer A, Chu DK, et al. Detection of 2019 novel coronavirus (2019-nCoV) by real-time RT-PCR. Euro Surveill. 2020 Jan;25(3).
57. de Wilde AH, Raj VS, Oudshoorn D, Bestebroer TM, van Nieuwkoop S, Limpens R, et al. MERS-coronavirus replication induces severe in vitro cytopathology and is strongly inhibited by cyclosporin A or interferon-α treatment. The Journal of general virology. 2013 Aug;94(Pt 8):1749-60.
58. Graham C, Seow J, Huettner I, Khan H, Kouphou N, Acors S, et al. Neutralization potency of monoclonal antibodies recognizing dominant and subdominant epitopes on SARS-CoV-2 Spike is impacted by the B.1.1.7 variant. Immunity. 2021 2021/06/08/;54(6):1276-89.e6.
59. Mootha VK, Lindgren CM, Eriksson K-F, Subramanian A, Sihag S, Lehar J, et al. PGC-1α-responsive genes involved in oxidative phosphorylation are coordinately downregulated in human diabetes. Nature Genetics. 2003 2003/07/01;34(3):267-73.
60. Subramanian A, Tamayo P, Mootha VK, Mukherjee S, Ebert BL, Gillette MA, et al. Gene set enrichment analysis: A knowledge-based approach for interpreting genome-wide expression profiles. Proceedings of the National Academy of Sciences. 2005;102(43):15545-50.
61. Aliee H, Massip F, Qi C, Stella de Biase M, van Nijnatten JL, Kersten ETG, et al. Determinants of SARS-CoV-2 receptor gene expression in upper and lower airways. medRxiv. 2020 Sep 2.
62. Sikkema L, Strobl D, Zappia L, Madissoon E, Markov N, Zaragosi L, et al. An integrated cell atlas of the human lung in health and disease. Preprint bioRxiv. 2022:2022.03.10.483747.
63. Newman AM, Liu CL, Green MR, Gentles AJ, Feng W, Xu Y, et al. Robust enumeration of cell subsets from tissue expression profiles. Nat Methods. 2015 May;12(5):453-7.